Akademisk avhandling för filosofie doktorsexamen

Hyperfine Structure Calculations for Highly Charged Hydrogen-Like Ions

— Investigations of nuclear charge and magnetization distributions

Martin G. H. Gustavsson

GÖTEBORGS UNIVERSITET
CHALMERS TEKNISKA HÖGSKOLA
Fysik och teknisk fysik
Atomfysik

Göteborg 2000

Hyperfine Structure Calculations for Highly Charged Hydrogen-Like Ions — Investigations of nuclear charge and magnetization distributions
Martin G. H. Gustavsson
ISBN 91-628-4567-5

Atomfysik
Fysik och teknisk fysik
Göteborgs universitet och Chalmers tekniska högskola
SE-412 96 Göteborg
Sweden
Tel: +46 (0)31-772 3273, Fax: +46 (0)31-772 3496

Chalmers reproservice
Göteborg, Sweden 2000

Hyperfine Structure Calculations for Highly Charged Hydrogen-Like Ions

— Investigations of nuclear charge and magnetization distributions

Martin G. H. Gustavsson

Atomfysik
Fysik och teknisk fysik
Göteborgs universitet och Chalmers tekniska högskola
SE–412 96 Göteborg

Abstract

The hyperfine structure is an example of a physical phenomenon where the detailed structure of the atomic nucleus is reflected in the electronic energy levels of the atom. The analysis of the hyperfine interaction between the electrons and the nucleus thus serves as a sensitive probe of the nuclear structure and basic physical principles. It is today possible to produce and store highly charged ions, enabling accurate spectroscopical investigations. This possibility has caused a large interest in the studies of hyperfine structure in these ions, where the sensitivity to nuclear and quantum electrodynamics (QED) effects is greatly enhanced. This thesis presents calculations of the contributions from nuclear charge and magnetization distributions to hyperfine structure (hfs) in highly charged hydrogen-like ions. The status and reliability of tabulated nuclear magnetic dipole moments are also discussed. The present work includes direct numerical solutions for the relativistic electronic wavefunction in realistic nuclear charge distributions. These wavefunctions are then used to evaluate the effect on the hfs for different nuclear magnetization distributions. In addition, wavefunctions for the valence nucleon were obtained as a first estimate of the magnetization distribution. The calculated values can be combined with previously known QED contributions to predict the total effect as a guide to experiments, and to compare the results when available. If the nuclear magnetization is sufficiently well known, the comparison provides a test of calculated QED values—if not, the comparison instead provides information about this distribution. Extracted information about the nuclear magnetization distributions constitute the main results presented in this thesis.

Keywords: hyperfine structure, hyperfine anomaly, nuclear charge distribution, nuclear magnetization distribution, Bohr-Weisskopf effect, nuclear magnetic dipole moment

Sammanfattning

Hyperfinstruktur är ett exempel på ett fysikaliskt fenomen där atomkärnans detaljerade struktur reflekteras i energinivåerna för atomens elektroner. Analysen av hyperfin växelverkan mellan elektronerna och kärnan tjänar därmed som en känslig indikator för kärnans struktur och grundläggande fysikaliska principer. Det är numera möjligt att framställa och lagra högt laddade joner och detta möjliggör noggranna spektroskopiska undersökningar. Detta har orsakat ett stort intresse för studier av hyperfinstruktur i högt laddade joner, då fenomenets känslighet för kärnfysikaliska och kvantelektrodynamiska (QED) effekter är ytterst förstärkta i dessa system. Denna avhandling presenterar beräkningar av bidragen från kärnans laddnings- och magnetiseringsfördelningar till hyperfinstrukturen i högt laddade joner. Statusen och tillförlitligheten hos atomkärnors uppmätta magnetiska dipolmoment behandlas också. Arbetet inkluderar direkta numeriska lösningar av relativistiska elektroniska vågfunktioner för realistiska kärnladdningsfördelningar. Dessa vågfunktioner har sedan använts till att bestämma påverkan av hyperfinstrukturen från olika kärnmagnetiseringsfördelningar. Dessutom har vågfunktioner för valensnukleoner beräknats som en första uppskattning av magnetiseringsfördelningen. De beräknade värdena kan kombineras med tidigare kända QED bidrag för att förutsäga den totala effekten som en riktlinje för experimentellt arbete, och för att jämföra med tillgängliga resultat när sådana finnes. Om magnetiseringsfördelningen är tillräckligt välkänd kan jämförelsen innebära ett test av beräknade QED värden, om inte ger jämförelsen istället information om fördelningen. Sådan extraherad information om magnetiseringsfördelningar utgör de huvudsakliga resultaten presenterade i avhandlingen.

List of Publications

This thesis is based on the work contained in the following papers, referred to by Roman numerals in the text:

I. Hans Persson, Sten Salomonson, Per Sunnergren, Ingvar Lindgren and Martin G. H. Gustavsson, A Theoretical Survey of QED Tests in Highly Charged Ions, *Hyperfine Interactions*, 108:3–17, 1997.

II. Martin G. H. Gustavsson and Ann-Marie Mårtensson-Pendrill, Four Decades of Hyperfine Anomalies, *Advances in Quantum Chemistry*, 30:343–360, 1998.

III. J. R. Crespo Lopez-Urrutia, P. Beiersdorfer, K. Widmann, B. B. Birkett, A.-M. Mårtensson-Pendrill and M. G. H. Gustavsson, Nuclear magnetization distribution radii determined by hyperfine transitions in the 1s level of H-like ions $^{185}Re^{74+}$ and $^{187}Re^{74+}$, *Physical Review A*, 57(2):879–887, 1998.

IV. Martin G. H. Gustavsson and Ann-Marie Mårtensson-Pendrill, Need for remeasurements of nuclear magnetic dipole moments, *Physical Review A*, 58(5):3611–3618, 1998.

V. Martin G. H. Gustavsson, Christian Forssén and Ann-Marie Mårtensson-Pendrill, Thallium hyperfine anomaly, *Hyperfine Interactions*, 127:347–352, 2000.

VI. Ann-Marie Mårtensson-Pendrill and Martin G. H. Gustavsson, *The Atomic Nucleus*, Handbook of Molecular Physics and Quantum Chemistry, chapter 5. John Wiley & Sons, 2000.

VII. Peter Beiersdorfer, Steven B. Utter, Keith L. Wong, Jerry A. Britten, Hui Chen, Clifford L. Harris, José R. Crespo López-Urrutia, Robert S. Thoe, Daniel B. Thorn, Elmar Träbert, Martin G. H. Gustavsson, Christian Forssén and Ann-Marie Mårtensson-Pendrill, Hyperfine Structure of Hydrogen-Like Thallium Isotopes, manuscript intended for *Physical Review A*.

A summary of these papers is given in Appendix A.

Contents

CHAPTER 1

Introduction

The hyperfine structure is an example of a phenomenon where the detailed structure of the atomic nucleus is reflected in the electronic energy levels in the atom. The analysis of the hyperfine interaction between the electrons and the nucleus and the resulting splitting of the electronic energy levels thus serves as a sensitive probe of the nuclear structure. Consequently, the hyperfine interaction has for a long time been used as a tool for the scrutiny of nuclear properties and basic physical principles. Hyperfine structure was discovered in the 1890s shortly after the invention of high resolution interference spectroscopy (interferometry). It affects atomic spectral lines, causing many of them to consist of closely spaced components. The hyperfine structure was first explained by W. Pauli as a result of the orientational potential energy of a magnetic dipole moment associated with the atomic nucleus in a magnetic field associated with the motion and spin of the atomic electrons.

A well-known atomic spectral line is the yellow one in the spectrum from sodium (Na). It has a wavelength of about 590 nm and dominates the light from sodium-vapour lamps, which are used as lighting for roads in several countries. A vapour lamp, also called an electric discharge lamp, consists of a transparent container within which a gas is energized by an applied voltage and thereby made to glow. The applied voltage accelerates electrons, which may collide with atoms in the gas and then transfer energy to the atoms. When sodium atoms in such lamps gain extra energy, the valence electron of an atom is excited from the ground state to an excited state. The atom then spontaneously decays from the excited state and the yellow light is emitted from atoms which undergo a transition from the first excited state back to

the ground state. With very simple equipment, i.e., a lamp and a grating or a prism, one can see that this main spectral line consists of two components known as the Fraunhofer D-lines, D_1 and D_2, and the wavelengths can be determined to 589.6 nm and 589.0 nm, respectively, by using slightly more advanced equipment. This separation is an example of the "fine structure" phenomenon and is illustrated in Fig. 1.1, which shows schematic line spectra for sodium. The fine structure is due to the existence of a magnetic coupling between the electronic spin and the electronic orbital angular momentum. This coupling splits the first excited state into two substates with different energy, giving the two different transition wavelengths. Continuing the study using equipment with even higher resolution each D line is found to consist of a doublet, i.e., two lines, with a separation of about 0.002 nm and this is an example of the *hyperfine structure phenomenon*. This splitting into doublets is due to a splitting of the ground state into two hyperfine levels. The first excited state is also split into hyperfine levels, causing the lines, d_{11} and d_{12}, of the D_1 doublet to consist of two components each and similarly causing the lines, d_{21} and d_{22}, of the D_2 doublet to consist of three components each. However, the hyperfine structure splitting of the first excited state is much smaller than the corresponding splitting of the ground state. Consequently, the separation between the components of the d lines is much smaller than the separation of the main D lines.

The first hypothesis, to explain the hyperfine structure (hfs) in atomic spectra, associated the effect with the presence of several isotopes. But hfs also was observed in studies of atoms having only one stable isotope, notably bismuth (Bi), so some additional hypothesis was needed to deduce an explanation. However, the presence of several isotopes does give a contribution to the spectrum, known as the isotope shift, of the same order of magnitude as the hfs. W. Pauli, in 1924, was the first to suggest that the hfs phenomenon is due to the presence of a magnetic coupling between the atomic nucleus and the electrons. Furthermore, he also predicted the fundamental features of the Zeeman and Paschen-Back effects for the hfs [1]. Three years later in a classic investigation, S. Goudsmit and E. Back succeeded in fitting a large part of the spectrum for Bi into a consistent scheme of energy levels and, by observing the Paschen-Back effect, in establishing unambiguously the angular momentum quantum number of the bismuth nucleus [2]. Improvement in spectroscopical techniques in the late 1920s gave new results for the hfs in the spectrum of, e.g., Na [3], Cs [4] and Rb [5]. These new results also made it possible for E. Fermi, in 1930, to perform the first quantum mechanical calculation of nuclear magnetic moments [6].

The hfs studies was then for a long time primarily used as a method for determination of nuclear multipole moments, specifically the magnetic dipole

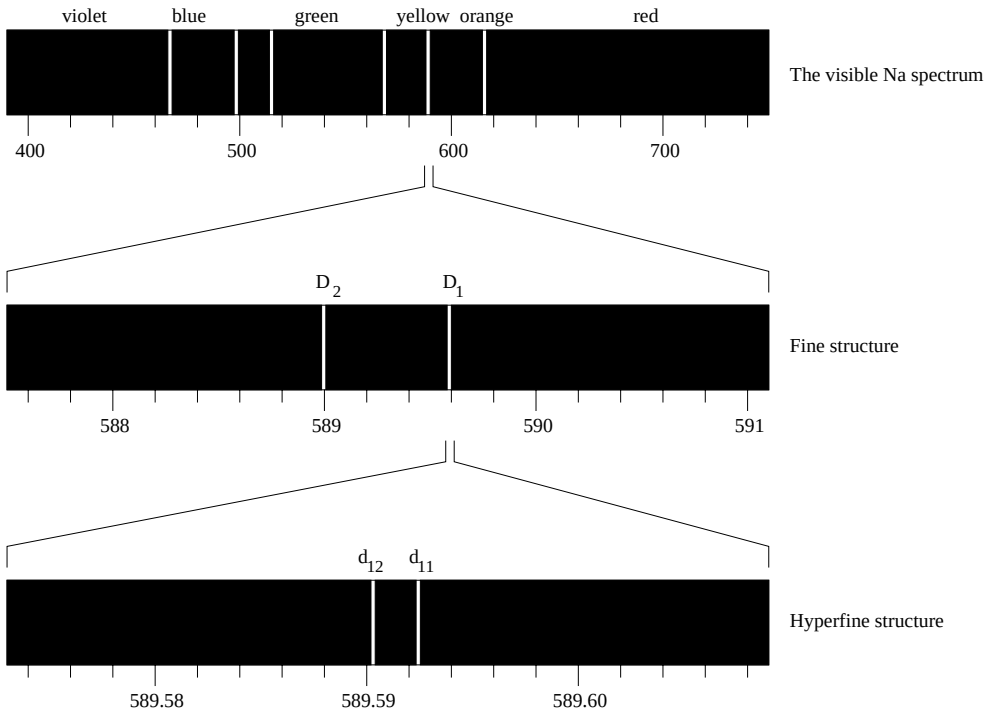

Figure 1.1: Schematic line spectra for Na with wavelength different ranges. The numbers below each spectrum indicates the wavelength in nm.

moments. Very precise measurements of the nuclear magnetic dipole moment have been performed also by other methods. This is, however, usually done on systems where the nuclei are shielded by the surrounding electron(s) and sometimes by a chemical environment. Corrections for this magnetic shielding are thus needed and this thesis contains a discussion about such corrections and the accuracy of nuclear magnetic dipole moment data.

The studies of hfs have continued and been developed. Theorists have learned to give better descriptions of the physics in an atom. D. R. Hartree and others developed so-called self-consistent calculations already in the late 1920s with the use of mechanical calculators [7]. Their calculations have since then been improved by the inclusion of several corrections for, e.g., electron correlation, relativity, extended nuclear charge distributions, extended nuclear magnetization distributions and quantum electrodynamics (QED). Correction factors based on analytical expressions can be useful and have been tabulated for many of the corrections [8]. Since the late 1960's the development of ever-more powerful computers has made it possible to perform more and more complete and accurate atomic physics calculations.

Accurate radio-frequency methods for hfs investigations was introduced by I. I. Rabi and further developed by N. F. Ramsey and others. The first motivation for doing these investigations was to get information about the nucleus, but such studies have also resulted in the development of atomic clocks and the present definition of the second*. One current application of atomic clocks is within the global positioning system, GPS [9].

It is today possible to create few-electron highly charged ions and to perform accurate spectroscopy on these extremely relativistic systems [10, 11]. Such work has been performed, e.g., at the ESR at GSI, Darmstadt and at the SuperEBIT at LLNL, California. These few-electron highly charged ions offer extremely strong electromagnetic fields, leading to a strong enhancement of the QED effects. However, not only QED effects but also effects from nuclear structure scale strongly with the nuclear field strength. The test of QED in strong fields may thus be limited by the known accuracy of nuclear properties. During recent years hfs measurements were reported for $^{165}Ho^{66+}$ [12], $^{185,187}Re^{74+}$ (Paper III), $^{203,205}Tl^{80+}$ (Paper VII), $^{207}Pb^{81+}$ [13], $^{209}Bi^{82+}$ [14] and $^{209}Bi^{80+}$ [15]. Furthermore, several theoretical investigations of these systems have been carried out, which included also QED corrections to all orders in $Z\alpha$, where Z is the nuclear charge in units of the elementary charge e and $\alpha \approx 1/137$ is the fine-structure constant. Some of the most recent studies were performed within our group here in Göteborg by Persson *et al.* [16] and Sunnergren *et al.* [17], as well as by Shabaev *et al.* [18] and Blundell *et al.* [19]. The aim of these studies is to perform comparisons between theory and experiments, which would give a test of QED in strong fields.

Definite conclusions about the validity of QED can, however, not always be drawn from the comparison between the experimental and the theoretical results since all nuclear parameters which describe the hyperfine interaction may not yet be known with sufficient accuracy. This thesis analyses the different uncertainties in these parameters and gives an overview of the status concerning the test of QED with use of hfs studies in highly charged ions. Whereas the nuclear charge distribution is, in general, sufficiently well known, the nuclear magnetization distribution is often quite uncertain. An alternative approach is to make use of the recent accurate QED calculations together with the experimental results in order to retrieve information about nuclear properties, in particular the magnetization distribution. This approach proves to be a fruitful way of using current available data and

*The second is at present defined in the following way: "The second is the duration of 9 192 631 770 periods of the radiation corresponding to the transition between the two hyperfine levels of the ground state of the cesium-133 atom."

is discussed and used in this thesis. The results from the latter approach constitute the main results presented in this thesis.

Thesis overview

This work treats the contributions to hfs from nuclear physics properties, i.e., extended charge and magnetization distributions and the nuclear magnetic dipole moments. Chapter 2 contains a brief discussion of general atomic theory and the theory of hfs. Chapter 3 continues with a qualitative discussion of the hfs phenomenon and a more quantitative discussion of the method used for hfs calculations. Such calculations usually start with first-order energy contributions, which in our work have been obtained by using direct relativistic numerical solutions for different nuclear charge distributions, which are discussed in Papers II and VI. In the next step we add contributions from the nuclear magnetization distributions as discussed in Paper II. Finally, QED contributions from the work of Sunnergren *et al.* [17] are added to achieve total theoretical values. The hfs is proportional to the nuclear magnetic dipole moment and the known accuracy, of the such moments, is thus essential for our studies. This topic is also treated in Paper IV. Chapter 4 contains results and discussions, i.e., a status report concerning the test of QED in hfs and extracted nuclear magnetization distribution data. Nuclear magnetization distribution radii are also discussed in Papers III, V and VII. It is demonstrated for thallium that data from measurements on neutral systems can be used for determination of isotopic differences in nuclear magnetization distributions and for accurate predictions of isotopic differences in the measurements on highly charged systems. Finally, Chapter 5 contains conclusions and an outlook.

Appendix A gives a summary of the papers included in the thesis, the theoretical description of the hyperfine interaction is treated Appendix B and Appendix C contains a short review over measurements and analyses of the nuclear magnetic dipole moment in ^{207}Pb.

CHAPTER 2

Atomic Theory

> "Who wanted to muck around the dirt, when you could be studying quantum mechanics?"
>
> Captain Janeway, STAR TREK: VOYAGER

This chapter contains a brief discussion of general atomic theory and the theory of hyperfine structure. More rigorous treatments can be found in several textbooks, e.g., Refs. [8, 20–24]. The theoretical description of the hyperfine interaction is treated in more detail in Appendix B. It must also be emphasized that the non-relativistic expressions in this chapter and Appendix B have not been used in the work presented in this thesis. They are only displayed for reasons of completeness and the connection to classical mechanics.

2.1 The Schrödinger equation

Non-relativistic calculations on atomic systems are usually based on the time-independent Schrödinger equation:

$$H\psi = E\psi\,, \tag{2.1}$$

where the wavefunction ψ and the energy E are the corresponding eigenfunction and eigenvalue of the Hamilton operator H. In the case of a one-electron atomic system with the nuclear charge Ze the non-relativistic Hamiltonian

for an infinitely heavy point-like nucleus is

$$H = -\frac{\hbar^2}{2m_\mathrm{e}}\nabla^2 - \frac{Ze^2}{4\pi\epsilon_0 r}\,,$$

where $\hbar$ is the Planck constant divided by 2π, m_e is the electron mass, ϵ_0 is the electric constant and r is the distance between the electron and the nucleus. It can be shown that the orbital angular momentum $\boldsymbol{l}$ is a constant of the motion for this central-field Hamiltonian and all other cases of spherical symmetry. Moreover, the angular part of the wavefunction is generally chosen to be represented by a spherical harmonic $Y^l_{m_l}(\theta,\phi)$, which is an eigenfunction of $\boldsymbol{l}^2$ and l_z, i.e., the projection of $\boldsymbol{l}$ along the z-axis. The eigenfunctions can then be written as

$$\psi_{nlm_l}(\boldsymbol{r}) = \frac{1}{r}P_{nl}(r)Y^l_{m_l}(\theta,\phi)\,,$$

where n denotes the principal quantum number, m_l is the eigenvalue of l_z and $\boldsymbol{r}$ stands for the spatial coordinates r, θ and ϕ. By inserting this wavefunction into the time-independent Schrödinger equation a differential equation for the radial functions $P_{nl}(r)$ is obtained. Furthermore, the energy eigenvalues of the one-electron case (for point-like nuclei) are found to be given by

$$E_n = -\frac{m_\mathrm{e}e^4}{2(4\pi\epsilon_0\hbar)^2}\frac{Z^2}{n^2}\,,$$

which, e.g., gives the ionization energy for the ground state of hydrogen ($Z = 1$, $n = 1$) to be about 13.6 eV.

Two disadvantages of using the Schrödinger equation in atomic physics calculations is that it does not incorporate relativity and the electronic spin $\boldsymbol{s}$, which is quite an important feature of the electron. The problem with the missing spin can, however, be circumvented by multiplying the wavefunction above with a Pauli spinor α or β. These spinors are chosen to be eigenfunctions of both $\boldsymbol{s}^2$ and s_z, and correspond to spin-up (α) and spin-down (β) states.

In the case of a many-electron atomic system the non-relativistic Hamiltonian can be written as

$$H = \sum_{i=1}^{N}\left(-\frac{\hbar^2}{2m_\mathrm{e}}\nabla_i^2 - \frac{Ze^2}{4\pi\epsilon_0 r_i}\right) + \sum_{i<j}^{N}\frac{e^2}{4\pi\epsilon_0 r_{ij}} + V_\mathrm{magn}\,,$$

where r_{ij} is the interelectronic distance. The first sum represents the contributions from the individual electrons, the second sum represents the Coulomb

repulsion among the electrons and the last term represents interaction of the spin of the electrons with magnetic fields produced by their spin and orbital motion (the so-called magnetic interaction, which, e.g., gives rise to the fine structure).

Not even the most powerful computers can deal with a wavefunction of the coordinates for all electrons of many-electron systems, and approximations must be introduced. In the the independent-particle model, the eigenfunction is written as a product of one-electron functions for N electrons. An additional, commonly used, approximation is the central-field model, allowing a separation of radial and angular parts. Within these approximations, the wavefunction can be obtained by iteration giving "self-consistent" potentials and wavefunctions, e.g., in the Hartree-Fock method, which has proven to be useful and is discussed in several textbooks, e.g., by Froese-Fischer [25] and by Lindgren and Morrison [21]. The single-configuration description of many-electron wavefunctions, although often useful as a first approximation, must be corrected if accurate results are needed. The "random phase approximation" (RPA) approach accounts for substitutions of one single-electron function at a time, and couplings between them. Correlation effects involve at least two electrons and can be treated in systematic ways using methods such as "configuration interaction" (CI), "multi-configurational Hartree-Fock" (MCHF) and "many-body-perturbation theory" (MBPT) and "coupled cluster approach" (CCA).

2.2 The Dirac equation

A relativistic treatment of atomic systems is provided by the Dirac equation which in Hamiltonian form is similar to the Schrödinger equation (2.1). The relativistic Hamiltonian for a one-electron system is given by

$$H = -i\hbar c\boldsymbol{\alpha}\cdot\nabla + \beta m_{\mathrm{e}}c^2 - \frac{Ze^2}{4\pi\epsilon_0 r}\,,$$

where c is the speed of light in vacuum. The Dirac (4×4) matrices $\boldsymbol{\alpha}$ and β are defined as

$$\boldsymbol{\alpha} = \begin{pmatrix} 0 & \boldsymbol{\sigma} \\ \boldsymbol{\sigma} & 0 \end{pmatrix}\,, \quad \beta = \begin{pmatrix} I & 0 \\ 0 & -I \end{pmatrix}\,,$$

where $\boldsymbol{\sigma}$ and I denote the Pauli spin-matrices and the identity matrix, respectively, i.e.,

$$\sigma_x = \begin{pmatrix} 0 & 1 \\ 1 & 0 \end{pmatrix}\,, \quad \sigma_y = \begin{pmatrix} 0 & -i \\ i & 0 \end{pmatrix}\,, \quad \sigma_z = \begin{pmatrix} 1 & 0 \\ 0 & -1 \end{pmatrix}\,, \quad I = \begin{pmatrix} 1 & 0 \\ 0 & 1 \end{pmatrix}\,.$$

The dimension of the Dirac matrices indicates that the eigenfunctions in total must have four components, but in the case of spherical symmetry it is convenient to write the eigenfunctions in terms of an upper and a lower component:

$$\psi_{n\kappa m}(\boldsymbol{r},\sigma) = \frac{1}{r}\begin{pmatrix} F_{n\kappa}(r)\chi_{\kappa m}(\theta,\phi,\sigma) \\ iG_{n\kappa}(r)\chi_{-\kappa m}(\theta,\phi,\sigma) \end{pmatrix},$$

where σ is the spin coordinate and the two-component spinor $\chi_{\kappa m}(\theta,\phi,\sigma)$ is a vector-coupled function of spherical harmonics and Pauli spinors. This relativistic description has thus an automatic inclusion of the spin phenomenon, furthermore, the sum of $\boldsymbol{l}$ and $\boldsymbol{s}$ gives the total electronic angular momentum $\boldsymbol{j}$. The parameter κ is given by

$$\kappa = l(l+1) - j(j+1) - \frac{1}{4} = \begin{cases} -\left(j+\frac{1}{2}\right) = -(l+1) & \text{for } j = l+\frac{1}{2} \\ j+\frac{1}{2} \;\; = l & \text{for } j = l-\frac{1}{2}\,. \end{cases}$$

The eigenvalues of the Dirac equation gives the *total energy* of the electron(s), i.e., the binding energy plus the rest mass energy $m_\mathrm{e}c^2$. In the one-electron case (for infinitely heavy point-like nuclei) the energy eigenvalue can be written as

$$E_{nj} = \frac{m_\mathrm{e}c^2}{\sqrt{1 + \dfrac{(Z\alpha)^2}{\left[n - \left(j+\frac{1}{2}\right) + \sqrt{\left(j+\frac{1}{2}\right)^2 - (Z\alpha)^2}\right]^2}}},$$

where the fine-structure constant is

$$\alpha = \frac{e^2}{4\pi\epsilon_0\hbar c}\,.$$

A series expansion of the energy gives

$$E_{nj} = m_\mathrm{e}c^2\left[1 - \frac{1}{2}\frac{(Z\alpha)^2}{n^2} - \frac{1}{2}\frac{(Z\alpha)^4}{n^4}\left(\frac{n}{j+\frac{1}{2}} - \frac{3}{4}\right) - \cdots\right],$$

where the second term is equal to the non-relativistic binding energy displayed above and the third term can be regarded as a relativistic correction to the kinetic energy and the spin-orbit interaction energy, i.e., the fine structure.

It can also be shown that for electrons with $E_{nj} \approx m_\mathrm{e}c^2$, e.g., in atomic systems with low nuclear charge, the lower component of the wavefunction

is "smaller" than the upper component by a factor of roughly $Z\alpha/2$. For this reason, the upper and lower components are respectively known as the *large* and *small* components of the Dirac wavefunction. Moreover, for the ground states of one-electron systems with low nuclear charge, the large (upper) component is essentially identical to the Schrödinger wavefunction multiplied by a Pauli spinor, i.e., $F_{1s}(r) \approx P_{1s}(r)$.

The relativistic treatment of many-electron atomic systems involves both computational and conceptual challenges. The need for two radial components for each electron increases the complexity of the calculation. In addition, the one-electron Dirac equation, itself, gives not only "positive-energy" solutions for electrons, but also "negative energy" solutions, corresponding to positrons. The presence of these solutions makes it necessary to account for virtual electron-positron excitations, leading to the theory of quantum electrodynamics (QED). In addition, the possibility of unwanted admixtures of negative energy compounds calls for particular care in the choice of basis set or numerical methods [26]. When such precautions are taken, the relativistic many-body problem can be treated by similar methods as the non-relativistic problem [27, 28]. The numerical basis set developed in our group has been applied also to the evaluation of radiative effects [29, 30].

2.3 Hyperfine structure

Hyperfine structure is a splitting of an atomic energy level caused by interactions between the electrons and electrodynamical moments of the nucleus. For electronic s-states, considered in this work, only the interaction with the nuclear magnetic dipole moment contributes. Generally, angular momenta of the electron(s) $\boldsymbol{J}$ and the nucleus $\boldsymbol{I}$ couple to form a total angular momentum $\boldsymbol{F}$, given by

$$\boldsymbol{F} = \boldsymbol{J} + \boldsymbol{I}$$

with the quantum numbers

$$\begin{aligned} F &= J + I, J + I - 1, \ldots, |J - I| \\ M_F &= F, F - 1, \ldots, -F\,. \end{aligned}$$

The Hamiltonian which describes the interaction between the electron(s) and the nuclear magnetic dipole moment can, following the discussion in Appendix B, be written in terms of an "effective" operator as

$$H_{\rm hfs} = \frac{A}{\hbar^2}\boldsymbol{J}\cdot\boldsymbol{I}\,,$$

where the A factor is called a *dipole interaction constant*. The A factor is, as also shown in Appendix B, the radial overlap of the electronic orbitals and the hyperfine operator times the nuclear g_I-factor and some well-known fundamental constants. The g_I-factor can be regarded as the magnitude of the nuclear magnetic dipole moment. In the non-relativistic limit, the hyperfine structure for an s-electron is described by a contact interaction and even in the relativistic case, the interaction takes place mainly in a region within or very close to the nucleus. The produced energy shift, from the effective operator above, is given by

$$E_{\text{hfs}} = \frac{A}{2}\left[F(F+1) - J(J+1) - I(I+1)\right] .$$

This implies that an atomic energy level is split into $(2I+1)$ hfs-levels if $I \leq J$ and $(2J+1)$ hfs-levels if $J \leq I$ and that the separation between the hfs-levels F and $F-1$ is equal to

$$\Delta E_{\text{hfs}} = AF .$$

For the s-states (and non-zero I) discussed in this work there are two hfs-levels present, since $J = 1/2$, with a separation given by

$$\Delta E_{\text{hfs}} = A(I + 1/2) . \tag{2.2}$$

The brief treatment of the hfs above will continue in the next chapter with a more detailed discussion regarding the physics close to the nucleus and our procedure for calculations of hfs in highly charged hydrogen-like ions. A more detailed treatment of the hfs operator is given in Appendix B.

CHAPTER 3

The Hyperfine Structure Phenomenon

This chapter continues the discussion from the previous chapter about the hyperfine structure phenomenon. It contains discussions about the physics close to the nucleus and about our procedure for calculations of hfs in highly charged hydrogen-like ions. In addition the dominating uncertainties are analysed.

3.1 Hydrogen and hydrogen-like bismuth

The present thesis deals with hfs in the ground state of highly charged hydrogen-like ions ($J = 1/2$). It can then be useful to start with a short review of the situation in ordinary hydrogen. The ground-state hfs in ^{1}H is due to the interaction between the angular momenta of the proton and the electron, giving the two F-levels 1 and 0, since $I = 1/2$. The transition between these two levels is well-known from radio astronomy and the frequency of the transmitted radiation is measured to be 1420 405 751.773(1) Hz [31], corresponding to a wavelength of about 21 cm and an energy separation of about 5.87 μeV. This extremely accurate result can unfortunately not be used in stringent tests of QED for weak fields, since the total theoretical predictions are much less accurate due to lack of information about the finite size and internal structure of the proton. A similar situation is also present in the cases of highly charged ions, as will be discussed in Chapter 4.

The hfs in ^{1}H is used in many applications; the hydrogen maser which has been used for the determination of the radiation frequency can also be

used as an accurate clock [9]. A particularly fascinating navigation feature, dependent on hydrogen masers used as accurate clocks, are the highly successful tours of the two Voyager spacecrafts through our planetary system. Another spectacular application of the hfs in ^{1}H is connected with the search for extraterrestrial intelligence. The radiation frequency lies in the microwave band, which is a rational choice for interstellar communications due to its good signal-to-noise properties [32]. Moreover, hydrogen is the most abundant element in the universe and this frequency must thus be known to every observer in a technically developed society.

In the case of the highly charged hydrogen-like ion $^{209}Bi^{82+}$ the ground-state hfs gives the two F-levels 5 and 4, since $I = 9/2$. Such ions were produced at GSI, Darmstadt, in 1994 and transitions between the two F-levels were then stimulated. The wavelength of the emitted radiation was measured to be about 244 nm [14], which corresponds to an energy separation of about 5.08 eV, i.e., a difference, with respect to the case of hydrogen, of 6 orders of magnitude!

There are several differences between the hfs in ^{1}H and in $^{209}Bi^{82+}$ and we will here qualitatively discuss these before the more quantitative approach in the next section. In the Bohr model, a hydrogen-like ion is treated as an electron orbiting the nucleus, like a planet in a solar system. The speed of the electron is $Z/137$ of the speed of light. For hydrogen, the nucleus can be approximated by a point charge, since the radius of the electron orbit is about 50 000 times larger than the radius of the nucleus. This "Bohr radius" is also the most probable distance from the nucleus in the quantum mechanical description. The hfs can, to a first approximation, be regarded as an effect caused by a point-like nuclear magnetic dipole in the presence of a magnetic field associated with the electron. The situation in $^{209}Bi^{82+}$ is quite different and a schematic picture is shown in Fig. 3.1. Relativity must be taken into account for the electron moving around the $Z = 83$ nucleus with a speed of about 83/137 of the speed of light. The radius of the electron orbit is inversely proportional to Z, and (in a non-relativistic extrapolation) 83 times smaller than for hydrogen. The nuclear radius, on the other hand, is nearly seven times larger, since it is proportional to $A^{1/3}$, where A is the mass number of the nucleus, which in this system equals 209. The radius for the orbit is then only about 90 times larger than the radius of the nucleus. In the quantum mechanical description, the orbital of the 1s electron has a substantial part located inside the nucleus, which can then no longer be approximated by a point-like charge.

The ^{209}Bi nucleus can, in a simple picture, be regarded as a ^{208}Pb nucleus with an extra outer proton. The ^{208}Pb nucleus is known to be "double-magic" where both protons and neutrons have particularly stable configurations with

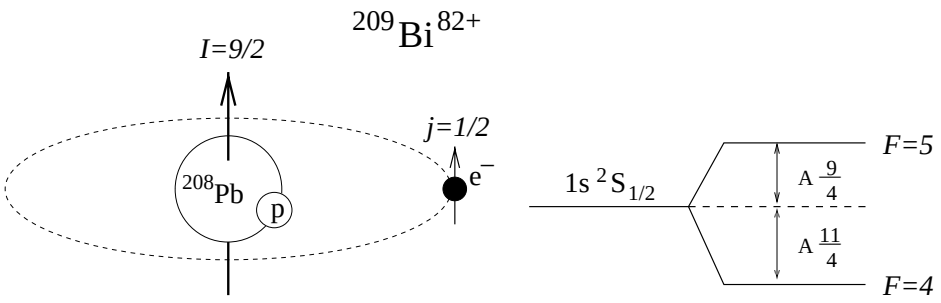

Figure 3.1: Schematic picture of hfs in $^{209}Bi^{82+}$.

a total angular momentum equal to zero. The angular momentum of the nucleus is then due to the spin and the orbital motion of the extra (odd) proton. The nuclear magnetic moment can still, in a first approximation, be regarded as a point-like dipole, but since the electron is quite close to the nucleus it will "feel" that the nuclear magnetic moment is distributed in space. Moreover, the electron will also "feel" that the major part of the nuclear magnetic moment has its origin in the small current loop from the orbital motion of the extra proton. On top of these differences compared with hydrogen, we also have the fact that effects from QED, such as self-energy and vacuum polarization, are greatly enhanced for highly charged ions. A schematic picture of the corrections needed to account correctly for hfs in highly charged ions is given in Fig. 3.2. Corrections due to nuclear recoil, arising due to the finite mass of the nucleus, will be not be considered here, since they are very small for the heavy systems discussed in this work, i.e., ^{165}Ho, ^{185,187}Re, ^{203,205}Tl, ^{207}Pb and ^{209}Bi. In the non-relativistic approximation of hfs, the recoil effect for a one-electron system is determined by the reduced mass correction $(1+m_e/M)^{-3}$, where M is the mass of the nucleus. The reduced mass correction gives, in the cases of the heavy systems discussed in this work, a relative reduction slightly less than 10^{-5}, which is an order of magnitude smaller than the experimental uncertainty.

3.2 Formal expressions

Fermi-splitting and relativity

The hfs is strictly speaking a relativistic phenomenon, since it depends on spin properties, but can for many system be treated in a "semi-classical" way. Fermi treated the hfs with a non-relativistic formalism in studies of alkali atoms, where he derived a approximate generalizations from the hydrogenic

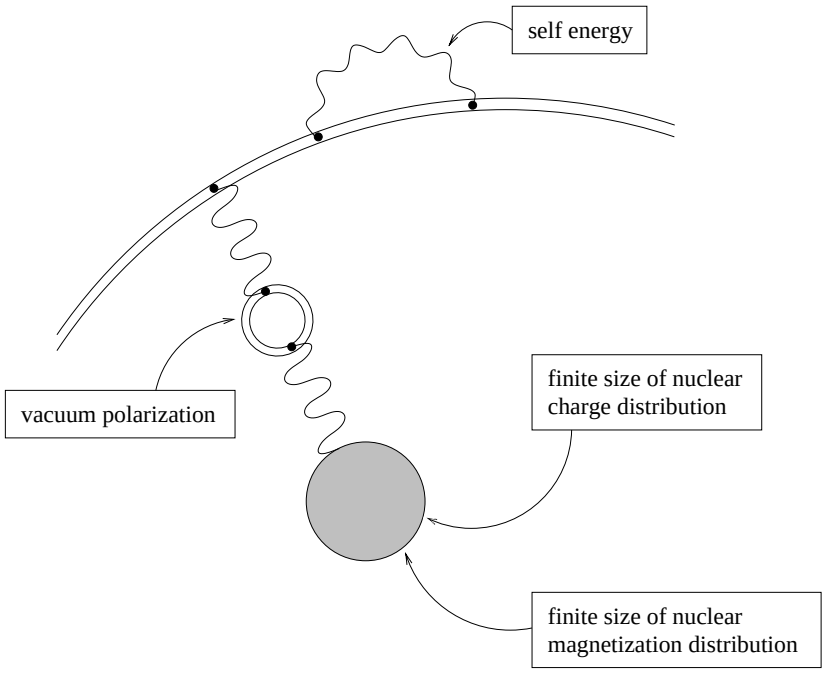

Figure 3.2: Schematic picture of the corrections to hfs beyond the relativistic first-order value for a point nucleus. The doubled line represents a bound electron, the wiggled line represents a virtual photon, the doubled ring represents a virtual electron-positron pair and the grey circle represents the nucleus.

case [6]. For a 1s electron in a hydrogen-like system with an infinitely heavy point-like nucleus the energy splitting is obtained by inserting known electron orbitals, giving

$$\Delta E_{\mathrm{F}} = \frac{4}{3}\alpha^4 Z^3 m_{\mathrm{e}} c^2 g_I \frac{m_{\mathrm{e}}}{m_{\mathrm{p}}} \left(I + \tfrac{1}{2}\right) ,$$

where $g_I = \mu_I / I\mu_{\mathrm{N}}$ is the nuclear g_I-factor, μ_I is the nuclear magnetic dipole moment, $\mu_{\mathrm{N}} = e\hbar/2m_{\mathrm{p}}$ is the nuclear magneton and m_{p} is the mass of the proton. This formula is also discussed in Appendix B and gives the so-called "Fermi-splitting". In the case of $^{209}\mathrm{Bi}^{82+}$ it gives a value of about 2.75 eV, which is 46% smaller than the experimental value. A relativistic treatment is, however, expected to improve the comparison due to the high speed of the electron.

Relativity can be taken into account by multiplying non-relativistic value with a relativistic correction factor [8, 33]. For an s electron, this has the value $1/\gamma(2\gamma - 1)$, where $\gamma = \sqrt{1 - (Z\alpha)^2}$. This expression holds for a

point-like nucleus and gives a hfs splitting for $^{209}Bi^{82+}$ of about 5.84 eV, which is 15% larger than the experimental value. Although the relativistic correction improves the comparison, a treatment beyond the point nucleus is clearly needed.

Nuclear charge distribution

The effect of the distribution of nuclear charge was analysed in pioneering works by Rosenthal, Breit [34] and others [35, 36] and it is sometimes called the "Breit-Rosenthal effect". The correction factor for the nuclear charge distribution can be written as $(1-\delta)$, where δ is a small number which depends mainly on the root-mean-square (rms) radius of the nuclear charge distribution, $\langle r_c^2\rangle^{1/2}$. By assuming a uniform spherical symmetric charge distribution and using the experimental value $\langle r_c^2\rangle^{1/2} = 5.519(4)$ fm for the nuclear charge distribution, δ can be calculated to be 0.110 in the case of $^{209}Bi^{82+}$ [37]. The relativistic first-order hfs energy-splitting in $^{209}Bi^{82+}$ for a uniformly charged nucleus then becomes about 5.20 eV, which is 2% larger than the experimental value. This treatment of the nuclear charge distribution can be improved by using a more "realistic" model in the calculation of δ.

In this work, we evaluate the hfs by using relativistic wavefunctions from a direct numerical solution of the Dirac equation for electronic s-states and an extended charge distribution, using the expression (discussed also in Appendix B)

$$\Delta E_1 = \frac{8}{3}\frac{e}{4\pi\epsilon_0 c} g_I \mu_N \left(I+\tfrac{1}{2}\right) \int_0^\infty F_{ns}\frac{1}{r^2} G_{ns} \mathrm{d}r \,. \tag{3.1}$$

Obviously, no additional correction factors for relativity and extended nuclear charge should be applied to this result. The convergence of the first-order value for the ground-state hfs in $^{209}Bi^{82+}$ is shown in Fig. 3.3.

Figure 3.4 shows experimental results for the radial variation of the charge density for different nuclei. These results show that the radial charge distribution is fairly constant from the centre of the nucleus to the diffuse surface, which has a thickness, called the "skin thickness", with a roughly constant value of 2.3 fm. Different models can be used to describe the nuclear charge distribution; we have used the two-parameter Fermi model and the model-independent Fourier-Bessel expansion to obtain a more realistic description. The Fermi model contains the basic features of the nuclear charge distribution described above and it is introduced in subatomic textbooks as "the simplest useful approximation". The Fourier-Bessel expansion is a *model-independent* expansion of the experimental data in terms of spherical Bessel functions, its uncertainties are, unfortunately, not trivial to handle. Both

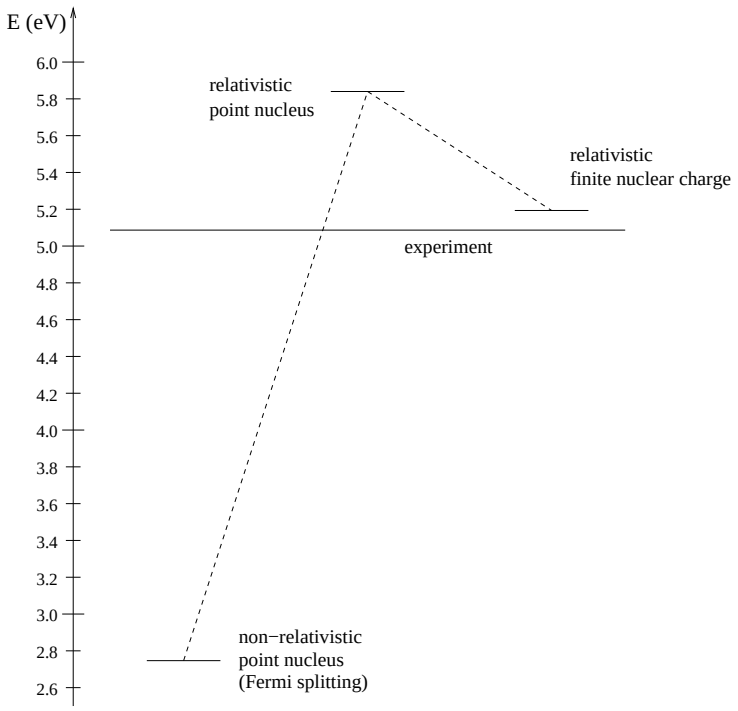

Figure 3.3: The values of the hyperfine splittings for various approximations compared with the experimental result for $^{209}Bi^{82+}$. The uncertainties in the values are too small to be displayed in this figure.

these distributions are described in more detail in Papers II and VI, and parameters for different nuclei can be found in tabulations such as Refs. [38, 39]. To summarize, we use a numerical solution of the Dirac equation for a realistic distribution of the nuclear charge and Eq. (3.1) to calculate our first-order value for the hfs energy-splitting in hydrogen-like systems.

Having obtained a first-order hfs value, we can now add the two final corrections for extended nuclear magnetization and for QED to get the total hfs energy-splitting, which can be written as

$$\Delta E_{\rm hfs} = \Delta E_1(1-\varepsilon) + \Delta E_{\rm QED}\,, \tag{3.2}$$

where $(1-\varepsilon)$ is the correction factor for an extended magnetization distribution of the nucleus.

Nuclear magnetization distribution and QED

The correction for an extended nuclear magnetization was first studied in an innovative work by A. Bohr and Weisskopf [40, 41] and is also called "the

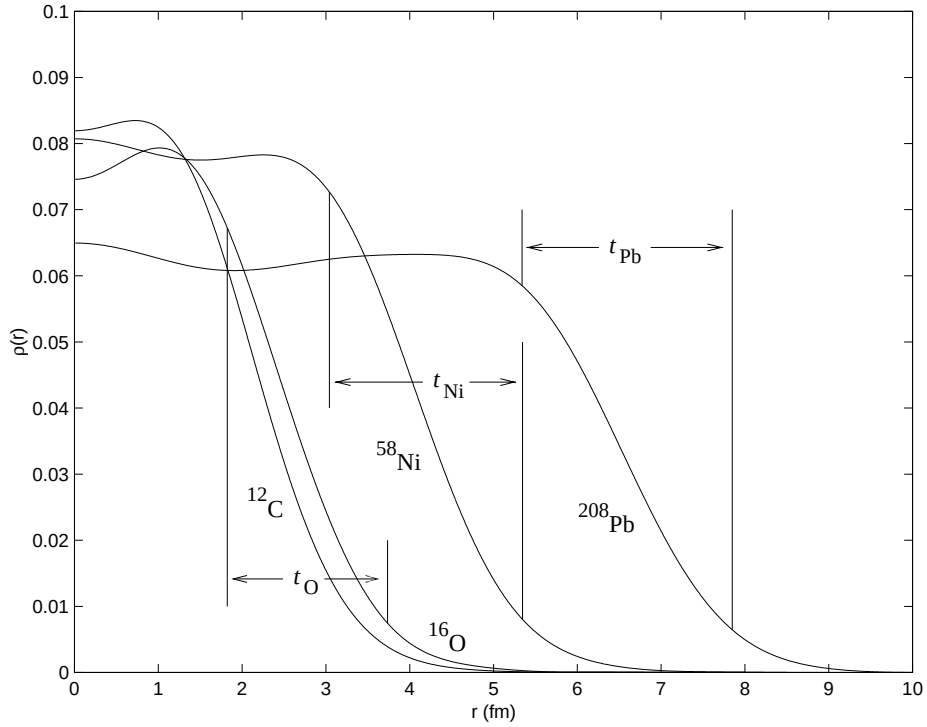

Figure 3.4: The radial charge distribution for several nuclei determined by electron scattering. The skin thickness t is shown for O, Ni and Pb; its value is roughly equal to 2.3 fm. These distributions were adapted from the tabulation by de Vries *et al.* [38].

Bohr-Weisskopf effect". Their work makes use of a correction parameter ε, which is described in more detail in Paper II, when replacing the magnetic point dipole approximation in Eq. (3.1) by a treatment including a distributed magnetization. This parameter is, however, not trivial to achieve due to the lack of information about the magnetization distribution. It is of course possible to assume a distribution, e.g., the uniform and Fermi models mentioned above or a shell model, where the magnetization is assumed to be localized on a spherical shell around the nucleus. The shell model is a fairly good assumption if the nuclear magnetization has its origin in the spin and orbital motion of an (outer) unpaired nucleon, but the problem of getting a radius of the shell remains.

Recently, three approaches for a theoretical *ab initio* determination of the Bohr-Weisskopf effect have been used. The simplest of these approaches is based on a solution of the Schrödinger equation for a nucleon in a Woods-Saxon potential, the solution gives the distribution for the unpaired nucleon

in the nucleus and the distribution is used to determine ε. This approach is explained in more detail in Paper V and in the work by Forssén [42], and has also been used by Shabaev [18]. A little more sophisticated approach, giving equivalent results for the hfs in leading order, is the "dynamical proton model" (DPM), where the odd proton of the Bi nucleus is treated as a Dirac particle bound in a Woods-Saxon potential. The first-order hfs in hydrogen-like Bi is then given as a vector-photon exchange between the electron and the proton. DPM was introduced by Labzowsky *et al.* [43] and has so far only been applied to the ground-state hfs in $^{209}Bi^{82+}$. The third and more complete approach is a many-body calculation with use of the "dynamic correlation model" (DCM) for one-hole nuclei. This approach is the only calculation of the Bohr-Weisskopf effect which includes many-body corrections and Tomaselli *et al.* have used it for studies of several systems [44, 45]. The terms included there for the nucleons correspond to those included in the "RPA" approach for electrons, and are found to give significant contributions. The results from these three approaches are summarized and discussed in Chapter 4.

In addition to the dominating electrostatic and hyperfine interactions with the nucleus, the electron also interacts with the radiation field, an interaction described by QED. The dominating QED corrections originate from the one-loop self-energy and vacuum-polarization effects, which are depicted by so-called Feynman diagrams, such as those shown in Fig. 3.5. The basic idea of QED is that every electromagnetic interaction is due to the exchange of virtual photons between electrically charged particles. A more thorough discussion is presented in several textbooks, e.g., by Mandl and Shaw [46] and by Peskin and Schroeder [47]. The one-loop QED effects for hfs have been calculated by different groups and the results are consistent [17–19]. We will here use the results from Sunnergren *et al.* [17, 48].

3.3 Uncertainties

Finally, when all corrections to the first-order hfs energy-splitting in a hydrogen-like system are discussed, it is convenient to return to the theoretical expression for the total hfs energy splitting:

$$\Delta E_{\mathrm{hfs}} = \mu_I \left[\frac{\Delta E_1}{\mu_I}(1-\varepsilon) + \frac{\Delta E_{\mathrm{QED}}}{\mu_I} \right] . \tag{3.3}$$

This formula is the same as Eq. (3.2) except for a factorization of the nuclear magnetic dipole moment μ_I. It is now important to consider the uncertainties in this expression and we will discuss below the uncertainty for each part, i.e.,

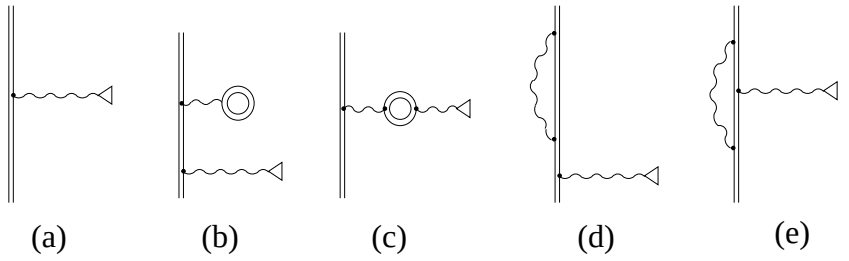

Figure 3.5: The Feynman diagrams representing the first-order interaction (a) and the one-photon radiative corrections (b)–(e) to the hyperfine splitting [17]. The double line represents a bound electron, the wiggly line represents a virtual photon, the triangle represents the magnetic interaction with the nucleus and the doubled ring represents a virtual electron-positron pair. The diagrams (b) and (c) are examples of vacuum polarization effects and (d) and (e) are examples of self-energy effects. The diagrams are constructed from well-defined rules and each can be rewritten as a mathematical expressions.

$\Delta E_1/\mu_I$, $\Delta E_{\rm QED}/\mu_I$, ε and μ_I. The first-order value ΔE_1 is given by Eq. (3.1) and this relation contains, except for $g_I = \mu_I/I\mu_{\rm N}$ and the components F and G of the electronic wavefunction, only well-known fundamental constants. An accurate treatment then shows that the dominating uncertainty in $\Delta E_1/\mu_I$ is due to uncertainties in the nuclear charge distribution, which in many cases is accurately determined by experiments and listed in tabulations. The QED correction has been calculated by different groups with results in agreement with each other and the relative uncertainty is estimated to be 1%. The uncertainty in the magnetization distribution parameter ε is a more difficult problem. In the case of the crude approach where the Schrödinger equation is solved for the unpaired nucleon, the result is assigned with a rather large uncertainty as discussed in Paper V and Refs. [18, 42]. The results from the dynamical correlation model for one-hole nuclei have been assigned with relatively small uncertainties [44, 45], but this nuclear many-body problem is difficult. Depending on the relative uncertainties of various parameters it can be more useful to turn the problem around. Instead of using the comparison between experiment and theory to perform a test of QED, one can combine calculated QED values and the experimentally determined $\Delta E_{\rm hfs}$ to obtain the parameter ε, giving in turn information about the nuclear magnetization distribution. This possibility is used and discussed in Papers III and VII and both possibilities will be discussed below.

Both ΔE_1 and $\Delta E_{\rm QED}$ are proportional to the magnetic dipole moment of the nucleus, and any uncertainty or error in the value of the nuclear mag-

netic dipole moment directly affects the total theoretical value. In all measurements of nuclear magnetic dipole moments an external magnetic field B_0 is applied. The external field induces a diamagnetic current density in the electron cloud surrounding the nucleus, and this leads to an induced magnetic field B' at the nucleus usually opposing the external field, so that the internal field at the nucleus becomes

$$B = B_0 - B'(0) = B_0 \left[1 - B'(0)/B_0\right] = B_0(1 - \sigma) \,.$$

We here introduce a magnetic shielding constant σ, which cannot be determined by varying the magnetic field because of the proportionality between B and B_0. Therefore, all experimentally determined nuclear magnetic dipole moments have to be corrected for the shielding effect. Theoretical estimates exist and are reasonably good for several free atomic systems where the magnetic shielding consists solely of a diamagnetic part. The claimed relative uncertainties of these diamagnetic corrections are usually not exceeding the order of 10^{-4}. However, many measurements of nuclear magnetic dipole moments have used the method of NMR, where the measurements are usually performed on molecules in an aqueous solution (or even a solid). The external magnetic field is then also shielded by the chemical environment, i.e., the molecular compound and the water, giving an additional paramagnetic shielding on top of the diamagnetic one. The variation of the magnetic shielding is called the chemical shift and it is difficult to evaluate except for simple molecular systems, since it depend on excitation energies in the molecule. For most elements, the chemical shift seems to be of the order of 10^{-3} or 10^{-4}, but can sometimes be larger. Shifts up to 1.3% have been observed in Co compounds [8, 49]. There is thus a need for accurate reassessments of the nuclear magnetic dipole moments in free atoms. The nuclear magnetic dipole moments used in this thesis are analysed and discussed in more detail in Paper IV.

3.4 Hyperfine anomaly

The results from hyperfine measurements have traditionally been presented in terms of A-factors. When comparing the hyperfine structure for two isotopes of the same element and electron configuration the electronic wavefunction can to a first approximation be assumed to be unchanged, and we would expect the ratio of A factors to be equal to the ratio of the corresponding nuclear g_I factors. A hyperfine anomaly is a deviation, Δ from this ratio,

and can be defined by

$$\frac{A_1}{A_2} = \frac{g_I^1}{g_I^2}\left(1 + {}^1\Delta^2\right) ,$$

and arise due to differences in the nuclear distributions. Accurate hfs measurements on neutral systems have over several decades provided many experimentally determined hyperfine anomalies. In general, magnetic shielding and chemical shift uncertainties do not affect anomaly determinations, since the nuclear moments for different isotopes of an element usually are measured simultaneously in the same experiment, and can be regarded as shielded by the same environment. The hyperfine anomaly is due to differences in nuclear charge and magnetization distributions. This implies that hyperfine anomaly measurements are sensitive tools for detection of differences in nuclear distributions. Moreover, hyperfine anomaly data for neutral systems can, as demonstrated in Chapter 4 and Papers V and VII, be used to predict the corresponding situation in highly charged systems.

3.5 Summary

Accurate comparisons between theoretical and experimental values of the hfs requires accurate values of the nuclear magnetic dipole moment and the calculations must include relativity, QED, the extended nuclear charge and magnetization distributions. In this work relativity and extended nuclear charge distribution are treated rigorously by solving the Dirac equation numerically. However, the nuclear charge distribution parameters can give rise to uncertainties in the energy splitting. The nuclear magnetic dipole moment can, unfortunately, be inaccurate (Paper IV), but it should be possible to perform a reassessment of the interesting magnetic moments giving a substantial reduction of the uncertainties. The remaining difficulties are then to calculate the corrections due to QED and the nuclear magnetization distribution.

The original aim for the experiments on hfs in highly charged ions was to perform tests of QED in strong fields, but that requires accurate corrections for the nuclear magnetization distribution. The determination of the correction for the nuclear magnetization distribution is a non-trivial problem, since our knowledge about the nuclear magnetization is limited. The QED contributions have been calculated by several groups with good agreement. Depending on the relative uncertainties of the various parameters, the experimental results can be used in different ways. One is to compare theoretical and experimental results in order to get a test of QED in strong fields, if the

nuclear magnetization distributions are sufficiently well known. In general, this is, however, not the case and it may instead be possible to combine calculated QED values and experimental hyperfine splittings in order to extract information about the nuclear magnetization. In the next chapter, both possibilities are considered.

CHAPTER 4

Results

This chapter contains our theoretical results for the ground-state hfs in the hydrogen-like systems $^{165}Ho^{66+}$, $^{185,187}Re^{74+}$, $^{203,205}Tl^{80+}$, $^{207}Pb^{81+}$ and $^{209}Bi^{82+}$. These results are used to interpret the experimental results in two ways: first, in an attempt to test the QED theory for highly charged ions and secondly, using calculated QED values to extract information about the nuclear magnetization distributions.

The first approach starts with relativistic calculations of the hfs for nuclear charge distributions described by the Fermi model. The next step is the calculation of the Bohr-Weisskopf effect, i.e., the corrections for extended nuclear magnetization distributions. Finally, previously calculated QED values are used to produce the total theoretical results for the hfs. The main uncertainty in these total values are the uncertainties in the Bohr-Weisskopf effect and it is found that, for most nuclei considered here, comparisons with the experimental values do not provide a sensitive test of the QED theory in strong fields.

The second approach turns the problem around and treats the Bohr-Weisskopf effect as an unknown parameter which can be obtained for by using experimental hfs values in addition to the theoretical QED contribution. Moreover, the extracted values for the Bohr-Weisskopf effect are used to get information about the nuclear magnetization distributions. The main uncertainty in the results by using this approach are the uncertainties in the values used for nuclear magnetic dipole moments.

In addition, it is demonstrated for Tl that data from measurements on neutral systems can be used for theoretical determinations of isotopic dif-

Table 4.1: Nuclear angular momenta, magnetic dipole moments and parameters for nuclear charge distributions described by the two-parameter Fermi model. The magnetic dipole moments are corrected for diamagnetic shielding and the given uncertainties contain possible chemical shifts (a more thorough discussion is given in Paper IV. The choice of charge distribution parameters are discussed in the text.

Nucleus	I	μ_I/μ_N	$\langle r_c^2\rangle^{1/2}$ (fm)	a (fm)	c (fm)
^{165}Ho	7/2	4.1767(53)	5.21(3)	0.57(1)	6.14(4)
^{185}Re	5/2	3.186(3)	5.39(1)	0.523(10)	6.49(2)
^{187}Re	5/2	3.219(3)	5.39(1)	0.523(10)	6.49(2)
^{203}Tl	1/2	1.6217(13)	5.463(5)	0.524(10)	6.59(2)
^{205}Tl	1/2	1.6379(13)	5.470(5)	0.524(10)	6.60(2)
^{207}Pb	1/2	0.5918(14)	5.497(2)	0.546(10)	6.60(2)
^{209}Bi	9/2	4.110(4)	5.519(4)	0.468(39)	6.76(7)

ferences in the nuclear magnetization distributions, which lead to accurate predictions of isotopic differences in measurements on highly charged ions.

This chapter is outlined as follows: the first approach, i.e., test of QED, is treated in Secs. 4.1–4.4, the second approach i.e., determination of nuclear magnetization, is treated in Sec. 4.5 and results for thallium, finally, in Sec. 4.6.

4.1 Nuclear charge distributions

The values for the first-order relativistic hfs energy splitting for an extended nuclear charge, $\Delta E_1/\mu_I$ in Eq. (3.3), have been calculated with the use of Eq. (3.1) and nuclear charge distributions described by the two-parameter Fermi model. The rms-radius $\langle r_c^2\rangle^{1/2}$ and the skin-thickness a are chosen as the distribution parameters and the uncertainty in these parameters totally dominates the estimated uncertainty in $\Delta E_1/\mu_I$. The parameters for ^{165}Ho, ^{203,205}Tl, ^{207}Pb and ^{209}Bi have been determined experimentally and the values used are given in the tabulation of de Vries *et al.* [38]. An interpolation of results for W and Os has been used for the case of ^{185,187}Re in the absence of experimentally determined parameters, as discussed in more detail in Paper III. The nuclear charge distribution parameters and magnetic dipole moments used are tabulated in Table 4.1. In addition, the half-density radius c for each nuclear charge distribution is also given. These radii can be regarded as the nuclear charge radii. The hyperfine interaction is sensi-

Table 4.2: Our values of $\Delta E_1/\mu_I$ calculated with use of Eq. (3.1) and nuclear charge distributions described by the two-parameter Fermi model. The nuclear charge distribution parameters were taken from Table 4.1. Note that the Bohr-Weisskopf effect is not include in these values. The QED values are taken from the work by Sunnergren *et al.* [17].

System	$\Delta E_1/\mu_I$ (eV/μ_N)	x_r (10^{-3} fm^{-2})	x_a (10^{-3} fm^{-2})	$\Delta E_\mathrm{QED}/\mu_I$ (eV/μ_N)
^{165}Ho^{66+}	0.5313(1)	−0.683	1.31	−0.002 587(3)
^{185,187}Re^{74+}	0.8775(1)	−0.925	1.73	−0.004 691(5)
^{203}Tl^{80+}	2.0378(2)	−1.16	2.15	−0.011 14(11)
^{205}Tl^{80+}	2.0376(2)	−1.16	2.15	−0.011 14(11)
^{207}Pb^{81+}	2.1524(1)	−1.20	2.22	−0.012 27(12)
^{209}Bi^{82+}	1.2628(2)	−1.25	2.25	−0.007 26(7)

tive to the electronic wavefunction close to the nucleus and changes in the nuclear charge density leads to changes in the hfs. The leading correction to the wavefunction is proportional to $\langle r_\mathrm{c}^2\rangle$, so any uncertainty in $\langle r_\mathrm{c}^2\rangle$ will lead to an uncertainty in the hfs, as further investigated in Paper II. The sensitivity to changes in the nuclear charge distribution is most easily seen by expressing $\Delta E_1/\mu_I$ in terms of changes in $\langle r_\mathrm{c}^2\rangle$ and a^2:

$$\frac{\Delta E_1}{\mu_I} = \frac{\Delta E_1^0}{\mu_I}\left[1 + x_r\delta\langle r_\mathrm{c}^2\rangle + x_a\delta a^2\right] ,$$

where x_r and x_a are the parameterization coefficients and the superscript 0 denotes the value for a reference distribution. It must also be emphasized that model-independent parameterizations in terms of changes in the moments $\langle r_\mathrm{c}^{2n}\rangle$ can and have been done in Paper II. These parameterizations are maybe our most important results concerned with the nuclear charge distribution. The hfs results are summarized in Table 4.2 together with values for x_r and x_a and the values for $\Delta E_\mathrm{QED}/\mu_I$ taken from Sunnergren *et al.* [17].

4.2 Calculations of the Bohr-Weisskopf effect

Paper II contains a discussion about the Bohr-Weisskopf effect and several formulæ are also given, but to obtain absolute values for the effect the nuclear magnetization distributions must be known. In analogy with the charge distribution, the leading correction to the electronic wavefunction is propor-

Table 4.3: Our calculated values of the nuclear magnetization radii and the Bohr-Weisskopf parameters ε for hfs in hydrogen-like ions. The relative uncertainties in ε are assumed to be 30%, except for the cases of ^{207}Pb and ^{209}Bi where the relative uncertainties are assumed to be 20% since these two nuclei are close to the double-magic nuclei ^{208}Pb. The nuclear potential parameters were taken from Rost [51].

Nucleus	Valence nucleon	Ground state	$\langle r_{\rm m}^2\rangle^{1/2}$ (fm)	ε (%)
^{165}Ho	proton hole	$2\,f_{7/2}$	5.66(79)	0.99(30)
^{185}Re	proton hole	$2\,d_{5/2}$	5.28(74)	1.18(35)
^{187}Re	proton hole	$2\,d_{5/2}$	5.28(74)	1.19(36)
^{203}Tl	proton hole	$3\,s_{1/2}$	5.26(74)	1.74(52)
^{205}Tl	proton hole	$3\,s_{1/2}$	5.27(74)	1.74(52)
^{207}Pb	neutron hole	$3\,p_{1/2}$	6.40(61)	4.29(86)
^{209}Bi	proton	$1\,h_{9/2}$	6.20(59)	1.31(26)

tional to the squared nuclear magnetization rms-radius $\langle r_{\rm m}^2\rangle$. We have performed model-independent parameterizations of ε in terms of the moments $\langle r_{\rm m}^{2n}\rangle$ and the coefficients for these parameterizations are given in Paper II. Attempts to determine nuclear magnetization distributions experimentally have been made, although results for heavy nuclei do not seem to have been achieved [50]. It is of course possible to assume that nuclear magnetizations are distributed, e.g., over a shell, but to obtain a quantitative estimation of ε we have used a simple single-particle model to obtain the distribution. We have in our model assumed that the nuclear magnetization is generated by an unpaired nucleon and we have then solved the Schrödinger equation for this nucleon in a Woods-Saxon potential, as described in more detail in Paper V and by Forssén [42]. Our results are in agreement with the results of Shabaev *et al.* [18], who used the same approach and potential and also have performed calculations with the inclusion of a spin-orbit (SO) term in the determination of ε, giving contributions well inside the stated accuracy. Both that work and ours used a nuclear Woods-Saxon potential with parameters from the work by Rost valid for nuclei in the lead region [51]. A summary of our theoretical results is given in Table 4.3.

Our results for ε are in Table 4.4 compared with the results from Shabaev *et al.*, the "dynamic correlation model" (DCM) calculations by Tomaselli *et al.* and the "dynamical proton model" (DPM). Our results are in agreement with the results, without SO-contribution, of Shabaev *et al.* and the discrepancies are probably due to their use of approximate formulas for the contribu-

Table 4.4: Summary of calculated Bohr-Weisskopf effects.

System	ε^a	ε (no SO)^b	ε (with SO)^b	ε (DPM)^c	ε (DCM)^d
$^{165}Ho^{66+}$	0.0099	0.0085	0.0089	—	0.0138
$^{185}Re^{74+}$	0.0118	0.0120	0.0122	—	0.0276
$^{187}Re^{74+}$	0.0119	—	—	—	0.0285
$^{203}Tl^{80+}$	0.0174	0.0177	0.0179	—	—
$^{205}Tl^{80+}$	0.0174	0.0177	0.0179	—	—
$^{207}Pb^{81+}$	0.0429	0.0419	—	—	0.0289
$^{209}Bi^{82+}$	0.0131	0.0133	0.0118	0.0131	0.0210

[a] This work.
[b] Shabaev *et al.* [18].
[c] Labzowsky *et al.* [43], Sunnergren *et al.* [17].
[d] Tomaselli *et al.* [45].

tions from the electronic wavefunction [37]. The results with SO-contribution of Shabaev *et al.* differ slightly from the results without SO-contribution, however, both this difference and the discrepancy with our values are notably smaller than the assumed uncertainties. It is also interesting that the DPM result for $^{209}Bi^{82+}$ is consistent with our result, relativistic effects on the nuclear charge distribution are thus negligible on this level of accuracy. The results from the DCM calculations, which include additional contributions, differ substantially from other results, pointing to the importance of nuclear many-body effects. These effects must thus be carefully investigated as mentioned above.

4.3 Comparison between theory and experiment

The total theoretical values of the ground-state hfs can now be obtained by using the following expression:

$$\Delta E_{\mathrm{hfs}} = \Delta E_1(1-\varepsilon) + \Delta E_{\mathrm{QED}}\,.$$

The values for ΔE_1 and ΔE_{QED} are obtained by multiplying the values for μ_I in Table 4.1 with the values for $\Delta E_1/\mu_I$ and $\Delta E_{\mathrm{QED}}/\mu_I$ in Table 4.2. The main contributor to the uncertainty of ΔE_1 is in general the uncertainty of μ_I. The values for ε are displayed in Table 4.3. The values for ΔE_1, ε, ΔE_{QED} and the total theoretical values are summarized and compared with the experimental results in Table 4.5. The comparison between our total

Table 4.5: Our total theoretical values of the ground-state hfs and the experimental results. The nuclear magnetic moments used are given in Table 4.5 and discussed in more detail in Paper IV. The major contributions to the uncertainties of total theoretical values are the uncertainties in the Bohr-Weisskopf effects, which were obtained with use of a Woods-Saxon potential as discussed in the text and in Paper V.

System	ΔE_1 (eV)	ε (%)	$\Delta E_{\rm QED}$ (eV)	$\Delta E_{\rm hfs}^{\rm theory}$ (eV)	$\Delta E_{\rm hfs}^{\rm exper.}$ (eV)
$^{165}Ho^{66+}$	2.2191(29)	0.99(30)	−0.010 81(11)	2.1863(72)	2.1645(6)[a]
$^{185}Re^{74+}$	2.7956(27)	1.18(35)	−0.014 94(15)	2.748(10)	2.7190(18)[b]
$^{187}Re^{74+}$	2.8245(27)	1.19(36)	−0.015 10(15)	2.776(10)	2.7450(18)[b]
$^{203}Tl^{80+}$	3.3047(27)	1.74(52)	−0.018 07(18)	3.229(17)	3.213 51(25)[c]
$^{205}Tl^{80+}$	3.3374(27)	1.74(52)	−0.018 25(18)	3.261(18)	3.244 10(29)[c]
$^{207}Pb^{81+}$	1.2738(30)	4.29(86)	−0.007 26(7)	1.212(11)	1.2159(2)[d]
$^{209}Bi^{82+}$	5.1903(51)	1.31(26)	−0.029 83(29)	5.092(15)	5.0840(8)[e]

[a] Crespo López-Urritia *et al.* [12].
[b] Crespo López-Urritia *et al.*, Paper III.
[c] Peter Beiersdorfer *et al.*, Paper VII.
[d] Seelig *et al.* [13].
[e] Klaft *et al.* [14]

theoretical and the corresponding experimental hfs results is also displayed in Fig. 4.1.

4.4 Test of QED or Nuclear Models?

The total theoretical and the corresponding experimental hfs results are in fair agreement, as shown in Table 4.5 and Fig. 4.1, since they agree within two standard deviations. The major contributions to the uncertainties in the theoretical results are the uncertainties in the nuclear magnetic dipole moment and in the Bohr-Weisskopf effect. The problems with the nuclear magnetic dipole moments are discussed in Paper IV, where it is stated that the uncertainties have been underestimated and that remeasurements are in many cases highly desirable. To theoretically determine the Bohr-Weisskopf effect accurately a good description for the magnetic properties of the nucleus is needed. Tomaselli *et al.* [44, 45] have used the DCM for one-hole nuclei to determine the Bohr-Weisskopf effect. Their method is the only one beyond the single-particle model and several effects which take place inside the nuclei

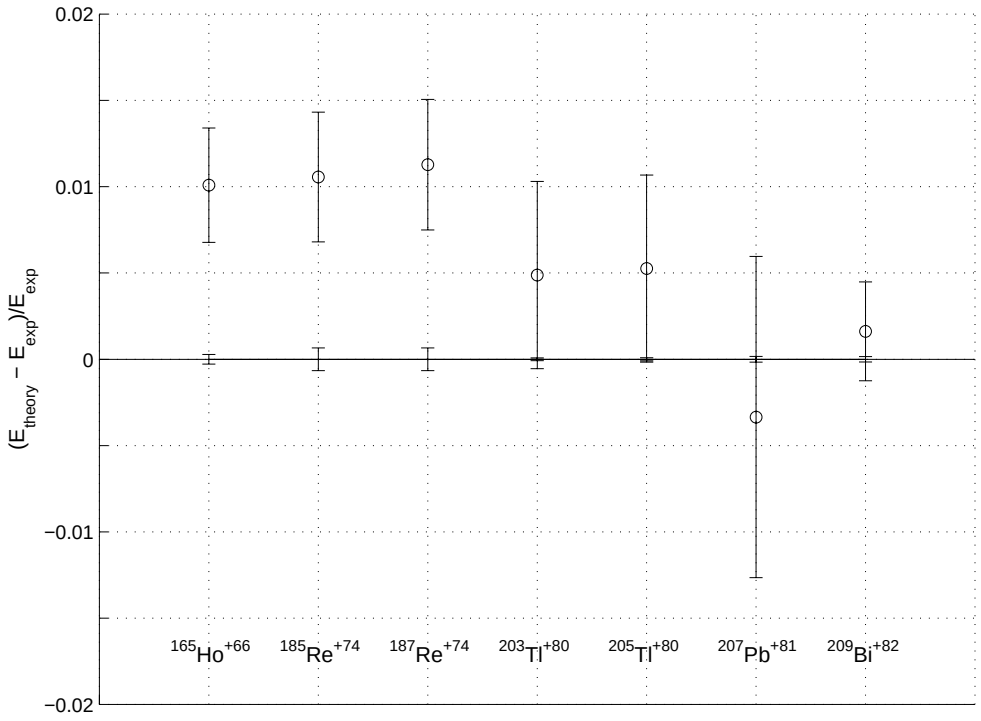

Figure 4.1: Comparison between our total theoretical hfs results (including relativity, extended nuclear charge, extended nuclear magnetization and QED) and the corresponding experimental hfs results. The circles indicate the relative differences between our values and the experimental ones, the small vertical lines on the horizontal zero line indicate the experimental error bars. All values are taken from Table 4.5.

are said to have been taken into account. However, their total hfs results do not coincide with the experimental ones, including the cases of $^{207}Pb^{81+}$ and $^{209}Bi^{82+}$. The nuclear magnetizations in ^{207}Pb and ^{209}Bi can be regarded as essentially due to single-particle effects since these two nuclei are one nucleon away from the double-magic nucleus ^{208}Pb, and the results from single-particle models gives fair results as discussed below. A more extensive theoretical and/or experimental determination of the nuclear magnetization distribution is thus needed.

Our simple determination of the Bohr-Weisskopf effect obtained by solving the Schrödinger equation for an unpaired nucleon in a Woods-Saxon potential, gives reasonably good results for the total hfs in the cases of $^{207}Pb^{81+}$ and $^{209}Bi^{82+}$. This situation is probably due to two reasons, first, the mag-

netization in these nuclei are essentially due to single-particle effects and secondly, the parameters of our model are valid. These parameters are expected to be relevant for nuclei close to the double-magic nuclei ^{208}Pb [51], i.e., ^{203,205}Tl, ^{207}Pb and ^{209}Bi in this work. The relative uncertainties of the Bohr-Weisskopf effect are set to 20% for both ^{207}Pb^{81+} and ^{209}Bi^{82+}, the effect on the total uncertainty is, however, different. In the case of ^{209}Bi^{82+} the parameter ε is small, giving a contribution to the total uncertainty smaller than the QED contribution, but in the case of ^{207}Pb^{81+} the parameter ε is large, giving a contribution to the total uncertainty exceeding the QED contribution.

Our total hfs results in the cases of ^{165}Ho^{66+} and ^{185,187}Re^{74+} are notably larger than the experimental results, but the nuclei in these systems are far from any double-magic nucleus and any single-particle model for the nuclear magnetization is only expected to give an order of magnitude estimate for these systems. For the cases of ^{203,205}Tl^{80+} the nuclei are close to the double-magic ^{208}Pb and our total hfs results coincides with the experimental ones. The agreement is not impressive, but our predictions were useful as a guide for the experimental work presented in Paper VII. The dynamical proton model (DPM) calculation of the Bohr-Weisskopf effect for ^{209}Bi^{82+} [17, 43], is in agreement with our result. The major difference between our single-particle model and DPM is the inclusion of relativity in the DPM, and the agreement implies that relativistic effects on the nuclear magnetization distribution are small.

A comparison between the hfs in hydrogen-like and lithium-like systems would make it possible to circumvent some problems with lack of information about nuclear parameters as recently proposed by Shabaev *et al.* [52]. This method is based on the idea that ε can be parameterized in terms of the moments $\langle r_{\rm m}^{2n} \rangle$, where the $\langle r_{\rm m}^{2} \rangle$-term is the leading one as discussed above. The Bohr-Weisskopf effect and the nuclear magnetization rms-radius for, e.g., a hydrogen-like system of one element can be extracted, as done in this work, and the nuclear magnetization radius can then be used to determine the Bohr-Weisskopf effect for the lithium-like system of the same element. Such work would, in combination with accurate nuclear magnetic dipole moments, provide tests of essentially only the QED contributions.

The original aim for the studies of hfs in highly charged H-like ions was to perform tests of the QED contributions, which constitute about 0.5% of the total hfs value for highly charged hydrogen-like ions. The case of ^{209}Bi^{82+} can possibly be regarded as a test of QED, since the theoretical value agrees within its 0.3% relative uncertainty with the experimental result. For the other cases studied this is not the case since the QED contribution is comparable in size with the total estimated uncertainty of the theory result.

Table 4.6: Experimental Bohr-Weisskopf effects and nuclear magnetization radii determined by a combination of the experimental results for $\Delta E_{\rm hfs}$ and the theoretical results for ΔE_1 and $\Delta E_{\rm QED}$. The uncertainties in the first parenthesis arise from the linear addition of uncertainties in the charge distribution and QED effects, and the second uncertainties from the addition of the uncertainties in the experimental hfs results and in μ_I, where the latter are dominating. The uncertainties in the third parenthesis in the cases of $\langle r_{\rm m}^2 \rangle^{1/2}$ relate to the magnetization model dependence.

System	ε (%)	$\langle r_{\rm m}^2 \rangle^{1/2}$ (fm)
^{165}Ho^{66+}	1.97(3)(15)	8.45(8)(44)(12)
^{185}Re^{74+}	2.20(2)(16)	7.51(4)(35)(10)
^{187}Re^{74+}	2.28(2)(16)	7.65(4)(34)(10)
^{203}Tl^{80+}	2.212(14)(80)	5.83(2)(13)(6)
^{205}Tl^{80+}	2.249(14)(79)	5.89(2)(12)(6)
^{207}Pb^{81+}	3.97(1)(25)	5.89(1)(23)(8)
^{209}Bi^{82+}	1.47(2)(11)	6.59(5)(29)(4)

However, the one-loop QED effects have been calculated by different groups and the results are consistent. It thus seems to be a rational choice to make use these calculations and using comparison between theory and experiment to extract information of the most uncertain parameter, i.e., the nuclear magnetization distribution.

4.5 Determination of nuclear magnetization radii

By turning the procedure around and solving for the Bohr-Weisskopf effect with use of the QED and experimental values, we can extract information about the nuclear magnetization distribution. This is an efficient and fruitful method of using the experimental data and it was done in Paper III for the cases of ^{165}Ho, ^{185,187}Re and ^{209}Bi and in Paper VII for the cases of ^{203,205}Tl, and all relevant formulæ can be found in Papers II and III. The revised nuclear magnetic moments presented in Paper IV imply, however, that also the extracted Bohr-Weisskopf effects and nuclear magnetization rms-radii must be revised, and the new results are given in Table 4.6.

A summary of our calculated and extracted nuclear magnetization rms-radii and ε parameters is given in Table 4.7 together with nuclear charge distribution parameters for comparison. This comparison shows that our

Table 4.7: Summary of our values for calculated and extracted nuclear magnetization rms-radii and ε parameters. The values are taken from Tables 4.3 and 4.6. Charge distribution parameters taken from Table 4.1 are included for comparison.

Nucleus	Charge distribution		Calculated values		Extracted values	
	$\langle r_c^2\rangle^{1/2}$ (fm)	c (fm)	ε (%)	$\langle r_m^2\rangle^{1/2}$ (fm)	ε (%)	$\langle r_m^2\rangle^{1/2}$ (fm)
^{165}Ho	5.21(3)	6.14(4)	0.99(30)	5.66(79)	1.97(18)	8.45(46)
^{185}Re	5.39(1)	6.49(2)	1.18(35)	5.28(74)	2.20(18)	7.51(37)
^{187}Re	5.39(1)	6.49(2)	1.19(36)	5.28(74)	2.28(18)	7.65(35)
^{203}Tl	5.463(5)	5.59(2)	1.74(52)	5.26(74)	2.212(81)	5.83(14)
^{205}Tl	5.470(5)	5.60(2)	1.74(52)	5.27(74)	2.248(81)	5.89(14)
^{207}Pb	5.497(2)	6.60(2)	4.29(86)	6.40(61)	3.97(26)	5.89(24)
^{209}Bi	5.519(4)	6.76(7)	1.31(26)	6.20(59)	1.47(13)	6.59(30)

approach to determine the nuclear magnetization rms-radii by using experimental hfs results and solving for the Bohr-Weisskopf effect gives three types of results. In the cases of ^{207}Pb and ^{209}Bi the values of ε and $\langle r_m^2\rangle^{1/2}$ are similar to our values from the estimation with use of our simple nuclear model, where the Schrödinger equation is solved for an unpaired nucleon in a Woods-Saxon potential. The results for $\langle r_m^2\rangle^{1/2}$ are in these cases slightly smaller than the half-density radius of charge distribution, respectively, indicating that the nuclear magnetizations are distributed over a shell in the external region of these nuclei. Moreover, our simple model thus describes the basic features of ^{207}Pb and ^{209}Bi, i.e., both ^{207}Pb and ^{209}Bi can be regarded as a double magic spherical symmetric ^{208}Pb nuclei with a odd neutron hole and a odd proton, respectively, distributed in the outer region of the nuclei.

The extracted results for ε of ^{165}Ho and ^{185,187}Re are about twice the values from the determination using our simple nuclear model, giving quite large values for $\langle r_m^2\rangle^{1/2}$, i.e., notably larger than the half-density radii of charge distributions. These large results can be due to nuclear magnetization distributions well outside the charge distributions and/or due to effects from deformed non-spherical nuclear structures. Better nuclear descriptions would hopefully clarify this situation and we can also conclude that a simple nuclear model is not suitable in these cases. The result for ^{165}Ho given here differs from previous result reported in Paper III due to the revised nuclear magnetic dipole moment.

The two stable thallium isotopes represent the third type of results. For these isotopes the extracted values for ε and $\langle r_m^2\rangle^{1/2}$ are similar to our values

from the calculation with use of our simple nuclear model, but the agreement is less than in the cases of ^{207}Pb and ^{209}Bi. Another difference compared to the cases of ^{207}Pb and ^{209}Bi is that the results for $\langle r_{\rm m}^2 \rangle^{1/2}$ are, in case of the thallium isotopes, slightly larger than the half-density radius of charge distribution, respectively, indicating that the nuclear magnetizations are distributed over a shell in the external region of the these nuclei. Our simple model thus gives an approximation for the basic features of the ^{203}Tl and ^{205}Tl nuclei and is also supported by previous calculations as discussed in Papers V and VII. However, as in the cases of ^{165}Ho and ^{185,187}Re better nuclear descriptions would hopefully be useful in the studies of the nuclear magnetization distribution. All our results for nuclear magnetization depend on the nuclear magnetic dipole moments used, and reassessments of the nuclear magnetic dipole moments are needed to get more accurate information of the nuclear magnetization.

The knowledge of nuclear magnetization distributions affects several problems in the external region between atomic and nuclear physics, as also discussed in Paper III. One important problem is the interpretation of atomic parity non-conservation experiments in chains of isotopes, which is limited by the uncertainty in the distribution of neutrons in the nucleus. Other problems are the search for P and T violation in atomic systems and to analyse data from nuclear anapole moment experiments, where a good understanding of nuclear wave functions is essential. We hope that our results can offer new calibrations in these studies.

4.6 Thallium hyperfine anomaly

The difference between the ground-state hyperfine separations in ^{205}Tl^{80+} and ^{203}Tl^{80+} is about 0.03 eV, as can be seen from Table 4.5, where the accuracy of the theoretical results are limited by the uncertainties in the Bohr-Weisskopf effect. However, as discussed in Chapter 3, measurements of hyperfine anomalies are sensitive tools for detection of differences in nuclear distributions. The $6p_{1/2}$ anomaly in neutral Tl is well known due to accurate measurements of the A-factors, 21 105.447(5) MHz and 21 310.835(5) MHz for ^{203}Tl and ^{205}Tl [53], respectively, and the nuclear magnetic moment ratio, $g_I(^{205}\mathrm{Tl})/g_I(^{203}\mathrm{Tl}) = 1.009\,836\,13(6)$ [54], giving $^{205}\Delta^{203} = -1.036(3) \times 10^{-4}$. The calculations by Mårtensson-Pendrill [55] shows that 91(1)% of this anomaly, i.e., $-0.944(11) \times 10^{-4}$, corresponds to the single-particle anomaly of a $p_{1/2}$ electron, and the increased value is due to many-body effects. For H-like systems only the single-particle effect is relevant. Furthermore, by scaling this single-particle contribution we can estimate the H-like 1s anomaly.

The effect from the differences in nuclear distributions on the anomaly can be written as

$$\Delta = \Delta_{\rm c} + \Delta_{\rm m} \,,$$

where the effect from the charge distribution can be expanded as

$$\Delta_{\rm c} = x_2 \delta\langle r_{\rm c}^2\rangle + x_4 \delta\langle r_{\rm c}^4\rangle + x_6 \delta\langle r_{\rm c}^6\rangle + \cdots \,,$$

and the effect from the magnetization distribution as

$$\Delta_{\rm m} = a_2 \delta\langle r_{\rm m}^2\rangle + a_4 \delta\langle r_{\rm m}^4\rangle + a_6 \delta\langle r_{\rm m}^6\rangle + \cdots \,.$$

The effect from the magnetization distribution is generally more complicated, but can be given this simple form in the case of Tl where the nuclear dipole moment can be regarded as originating from the spin of the unpaired 3s proton. The basic features of nuclear charge distributions can be described by a Fermi model as discussed previously, and the hyperfine anomaly due to a difference in charge distribution can thus be written as

$$\Delta_{\rm c} = x_r \delta\langle r_{\rm c}^2\rangle + x_a \delta a^2 \,,$$

where the parameters x_r and x_a in case of the single-particle effect are given in Table 4.8 for states of 1s in H-like Tl and $6p_{1/2}$ in neutral Tl. Engfer *et al.* [56] have from experimental data of muonic isotope shifts derived values for $\delta\langle r_{\rm c}^2\rangle$ by assuming Fermi distributions with $\delta a = 0$. Their result for the difference between ^{205}Tl and ^{205}Tl is $\delta\langle r_{\rm c}^2\rangle = 0.115(3)$ fm^2, giving $\Delta_{\rm c} = -0.897(23) \times 10^{-4}$ for 1s in H-like Tl and $\Delta_{\rm c} = -0.245(6) \times 10^{-4}$ for the single particle effect of $6p_{1/2}$ in neutral Tl.

The hyperfine anomaly due to a difference in magnetization distribution can, following Mårtensson-Pendrill [55], be rewritten in a more compact way:

$$\Delta_{\rm m} = a_2 \lambda_{\rm m} \,,$$

where

$$\lambda_{\rm m} = \delta\langle r_{\rm m}^2\rangle \left(1 + \frac{a_4}{a_2}\frac{\delta\langle r_{\rm m}^4\rangle}{\delta\langle r_{\rm m}^2\rangle} + \frac{a_6}{a_2}\frac{\delta\langle r_{\rm m}^6\rangle}{\delta\langle r_{\rm m}^2\rangle} + \cdots\right) .$$

The parameters a_2, a_4 and a_6 are given in Table 4.8 for 1s in H-like Tl and for the single-particle effect of $6p_{1/2}$ and 7s in neutral Tl. By using the above values of Δ and $\Delta_{\rm c}$ for the single-particle effect of $6p_{1/2}$ $\Delta_{\rm m}$ is determined to be $-0.699(13) \times 10^{-4}$, which corresponds to $\lambda_{\rm m} = 0.299(5)$ fm^2. The quantities a_4/a_2 and a_6/a_2 have very small variations for the states studied,

Table 4.8: Hyperfine anomaly parameters for the single-particle effect in Tl due to differences in nuclear charge and magnetization distributions.

	1s in H-like Tl	$6p_{1/2}$ in neutral Tl	7s in neutral Tl
x_r (10^{-3} fm^{-2})	−0.780	−0.213	—
x_a (10^{-3} fm^{-2})	0.513	0.143	—
a_2 (10^{-4} fm^{-2})	−7.73	−2.34	−8.39
a_4 (10^{-6} fm^{-4})	3.32	0.985	3.62
a_6 (10^{-9} fm^{-8})	−8.91	−2.66	−9.83
a_4/a_2 (10^{-3})	−4.29	−4.21	−4.32
a_6/a_2 (10^{-5})	1.15	1.14	1.17

making the $\lambda_{\rm m}$ parameter possible to use also for 1s in H-like Tl. Moreover, the change in magnetization can also be estimated to be $\delta\langle r^2_{\rm m}\rangle = 0.38(1)$ fm^2.

By using the analogy with the anomaly for $6p_{1/2}$ in neutral Tl, the 1s anomaly in H-like Tl due to a difference in magnetization distribution is found to be $-2.31(4) \times 10^{-4}$ giving a total hyperfine anomaly of $-3.21(5) \times 10^{-4}$. Using the ratio of the g_I-factors the energy ratio corresponding to our calculated hyperfine anomaly for 1s in H-like Tl is 1.009 511(5). To obtain an energy difference from this energy ratio we use our total hfs result for $^{203}Tl^{80+}$ giving an energy difference of 0.030 71(16) eV and a corresponding transition-wavelength difference of 3.617(19) nm. The recently measured values of 0.030 59(29) eV and 3.638(35) nm agrees with the calculated results as also discussed in Paper VII.

CHAPTER 5

Conclusions and Outlook

We have in this work performed calculations of the hfs in the ground state of the hydrogen-like ions $^{165}Ho^{66+}$, $^{185}Re^{74+}$, $^{187}Re^{74+}$, $^{203}Tl^{80+}$, $^{205}Tl^{80+}$, $^{207}Pb^{81+}$ and $^{209}Bi^{82+}$. The total hfs results for $^{207}Pb^{81+}$ and $^{209}Bi^{82+}$ are in fair agreement with experiment, but reassessments of nuclear magnetic dipole moments are needed to achieve good tests of the QED theory. This fair agreement indicates that the nuclear magnetizations for the systems considered are relatively well described by a single-particle model. Such a model is, however, not suitable for ^{165}Ho and $^{185,187}Re$, with their more complex nuclear structure. The discrepancies between theory and experiment point to a need for descriptions, which are better and more accurate in predicting nuclear structure, in particular the Bohr-Weisskopf effect. For $^{203}Tl^{80+}$ and $^{205}Tl^{80+}$ a single-particle model was expected to describe most of the nuclear magnetization for these single-valence nuclei. Our total hfs results were helpful in the experimental search for hfs transitions. The quite recent experimental results indicate that the magnetization distribution is larger than indicated by the nuclear single-particle calculation. Our calculated isotopic energy and wavelength differences for the hfs in the stable thallium isotopes are more accurate and agree with recent experimental results.

We have also used the experimental hfs results and the QED calculations to extract nuclear magnetization distribution radii. In addition to our results for ^{203}Tl, ^{205}Tl, ^{207}Pb and ^{209}Bi, where the magnetization can be regarded as located in the outer part of nucleus, we have unexpected results for ^{165}Ho, ^{185}Re and ^{187}Re. The results for these three nuclei are notably larger than the charge distribution radii. Our determined magnetization radii will hopefully

stimulate work for better descriptions of nuclear magnetization properties. They may also be used for calibration in studies in the region of overlap between atomic and nuclear physics, where, e.g., neutron distributions and nuclear wavefunctions are needed. One of these studies could be the search for atomic parity non-conservation.

The theoretical hfs determinations use nuclear parameters as input. Refined measurements of nuclear magnetic dipole moments and better descriptions of the nuclear magnetization are needed to fulfill the original aim of testing the QED effects in the cases of $^{203,205}Tl^{80+}$, $^{207}Pb^{81+}$ and $^{209}Bi^{82+}$. We hope that our accurate determination of the nuclear magnetization distribution radii will provide incentive for other theorists in their on-going development of more accurate methods for studying nuclear structure.

Acknowledgements

First of all I want to express my gratitude to Prof. Ann-Marie Mårtensson-Pendrill. I owe her many thanks for her highly valuable guidance and support during my time as a graduate student.

Prof. Ingvar Lindgren's willingness to help and share his great knowledge in many clarifying and helpful discussions is gratefully acknowledged. Prof. Eleanor Campbell has also contributed with help and suggestions.

From Docent Sten Salomonson and Docent Hans Persson I have learned a lot during our discussions about both general and quantum physics. I am also in debt to Dr. Håkan Warston for his introduction and help related to computers. I have shared many memorable moments and travels with Dr. Per Sunnergren and Björn Åsén. I am very grateful for their help and they have also become very good and much appreciated friends of mine. I also want to acknowledge that some parts of the presented work were done in close collaboration with Christian Forssén. During the last years I have shared many pleasant moments with Dr. Stefan M. Schneider, with whom I have discussed not only physics but also wine, music and literature. I also want to thank present and previous members of the atomic physics group and molecular physics group, for creating a nice atmosphere.

Finally, I want to acknowledge the very helpful support from my wife Anna, my parents and my friends, thank you for being there when I have needed you.

APPENDICES

APPENDIX A

Summary of Papers I–VII

This thesis is based on work reported in seven different papers, referred to by Roman numerals in the text. A summary of these papers follows below.

Paper I

This paper was published in a volume of Hyperfine Interactions devoted to the proceedings of the "2nd Euroconference on Atomic Physics with Stored Highly Charged Ions". It presents and discusses recent progress in precision tests of QED in strong nuclear fields. The discussion is focused on theoretical comparisons with experiments on the 1s Lamb-shift in H-like uranium, the two-electron Lamb-shift in He-like ions, the hyperfine structure of H-like bismuth and the bound-electron g-factor in H-like ions. My personal contributions were concentrated to the effect of the nuclear charge distribution in the cases of the 1s Lamb-shift in H-like uranium and the hyperfine structure of H-like bismuth.

Paper II

This paper was published in a volume of Advances in Quantum Chemistry dedicated to Prof. Ingvar Lindgren on the occasion of his 65th birthday. It gives a brief review over hyperfine structure studies, including work performed in Göteborg. The major sections discus nuclear charge and magnetization distributions in some detail and gives also several useful relations. The results are presented in terms of moments, thereby displaying directly

the sensitivity and emphasizing the need for a better understanding of nuclear wavefunctions.

Three small errors are present in this paper:

- page 350, FIG. 2, values for E/μ_I are given on the vertical axis instead of A/g_I as stated in the caption. In this case are these quantities related by $A/g_I = \frac{5}{6}E/\mu_I$,
- page 353, the expression for $\kappa_L(R)$ contains the parenthesis $(1-r/R^3)$, which should read $(1-r^3/R^3)$,
- page 358, Ref. [4], the year "(19451)" should read "(1951)".

Paper III

This article is a joint paper of experimental work performed at Lawrence Livermore National Laboratory and theoretical work performed in Göteborg. The experimental part reports that the wavelengths of the hyperfine transitions in the ground state of the two isotopes $^{185}Re^{74+}$ and $^{187}Re^{74+}$ were measured to be (4560.5 ± 3) Å and (4516.9 ± 3) Å, respectively, using emission spectroscopy in an electron beam ion trap. After applying appropriate corrections for the nuclear charge distribution and QED effects, a Bohr-Weisskopf effect of $\varepsilon = 2.23(9)\%$ and $2.30(9)\%$ are found for ^{185}Re and ^{187}Re, respectively. The radius of the nuclear magnetization distribution for ^{185}Re and ^{187}Re are then extracted to be $\langle r_m^2\rangle^{1/2} = 7.57(32)$ fm and $\langle r_m^2\rangle^{1/2} = 7.69(32)$ fm, respectively, considerably larger than the nuclear charge distribution radius. The parameter ε and nuclear magnetization distribution radius are also extracted for $^{165}Ho^{66+}$ and $^{209}Bi^{82+}$. The Bohr-Weisskopf effect in hydrogen-like ions is found to be a sensitive probe of the nuclear magnetization distribution, especially for cases where the charge distribution and magnetic moments are accurately known.

Paper IV

The aim for this paper was to point out the need for a reassessment of tabulated nuclear magnetic dipole moments as prompted by recent experiments on the ground-state hyperfine structure in highly charged hydrogen-like systems. This work gives an overview of the magnetic dipole moments for the nuclei of interest, i.e. ^{165}Ho, ^{185,187}Re and ^{203,205}Tl, ^{207}Pb and ^{209}Bi, including corrections for diamagnetic shielding and discussions of chemical shifts. It is found that the present uncertainties in the nuclear magnetic dipole moment limit the interpretation of the accurate experimental hyperfine structures for these systems.

Paper V

This paper was published in a volume of Hyperfine Interactions devoted to the proceedings of the "1st Euroconference on Atomic Physics at Accelerators". It considers the effects of the nuclear magnetization distribution on the hyperfine structure and briefly presents a solution of the Schrödinger equation for a nucleon in a Woods-Saxon potential. It also considers the isotopic differences in thallium and the difference in energy-splitting due to hyperfine structure for $^{203}Tl^{+80}$ and $^{205}Tl^{+80}$, respectively, is found to be 0.031 04(1) eV, which corresponds to a transition-wavelength difference of 3.640(1) nm. This prediction relies on accurate data for neutral Tl and thus has a uncertainty well below the expected experimental error bars.

Paper VI

This work is an invited chapter in the forthcoming "Handbook of Molecular Physics and Quantum Chemistry". The title is "The Atomic Nucleus" and it is mainly a review over nuclear charge distributions and the effects on atomic properties.

Paper VII

This article is a joint paper of experimental work performed at Lawrence Livermore National Laboratory and theoretical work performed in Göteborg. The experimental part reports that the hyperfine splitting of the 1s ground state of hydrogen-like Tl has been measured for the two stable isotopes using emission spectroscopy in the SuperEBIT electron beam ion trap, giving 3858.22 ± 0.30 Å for $^{203}Tl^{80+}$ and 3821.84 ± 0.34 Å for $^{205}Tl^{80+}$ with a wavelength difference $\Delta\lambda = 36.38 \pm 0.35$ Å, consistent with estimates based on hyperfine anomaly data for neutral Tl. By using previously determined nuclear magnetic moments and applying appropriate corrections for the nuclear charge distribution and radiative effects, the experimental splittings can be interpreted in terms of nuclear magnetization radii $\langle r_m^2 \rangle^{1/2} = 5.83(14)$ fm for ^{203}Tl and $\langle r_m^2 \rangle^{1/2} = 5.89(14)$ fm for ^{205}Tl. These values are 10% larger than derived from single-particle nuclear magnetization models, and are slightly larger than the corresponding charge distributions.

APPENDIX B

The Hyperfine Interaction Operator

A brief discussion of perturbations and matrix elements is given below. More thoroughly discussions can, e.g., be found in the textbooks by Jackson [57] and Lindgren and Morrison [21] and the article by Lindgren and Rosén [58].

B.1 Non-relativistic perturbation

The classical Hamilton function for a particle moving in some potential energy field $V(\boldsymbol{r})$ is

$$H = \frac{1}{2m}\boldsymbol{p}^2 + V(\boldsymbol{r})\,,$$

where m is the mass of the particle and $\boldsymbol{p}$ is the linear momentum. In presence of an electric and magnetic field, $\boldsymbol{E}$ and $\boldsymbol{B}$, derivable from a scalar and a vector potential, ϕ and $\boldsymbol{A}$:

$$\boldsymbol{E} = -\nabla\phi\,, \quad \boldsymbol{B} = \nabla \times \boldsymbol{A}\,,$$

the Hamiltonian becomes

$$H = \frac{1}{2m}(\boldsymbol{p} - q\boldsymbol{A})^2 + V(\boldsymbol{r}) + q\phi\,,$$

where q is the charge of the particle. The corresponding quantum mechanical Hamilton operator is given by

$$H = \frac{1}{2m}(-i\hbar\nabla - q\boldsymbol{A})^2 + V(\boldsymbol{r}) + q\phi\,, \tag{B.1}$$

since the quantity $\boldsymbol{p}$ is represented by the operator $-i\hbar\nabla$. The operators ∇ and $\boldsymbol{A}$ commute in Coulomb gauge since $\nabla \cdot \boldsymbol{A} = 0$ and the Hamiltonian can thus be rewritten as

$$H = -\frac{\hbar^2}{2m}\nabla^2 + V(\boldsymbol{r}) + q\phi + i\frac{\hbar q}{m}\boldsymbol{A}\cdot\nabla + \frac{q^2}{2m}\boldsymbol{A}^2\,.$$

The first two terms is recognized as the zero-field Hamiltonian, the third term gives the perturbation from an electric field, the fourth term scales linearly with $\boldsymbol{A}$ and is called *paramagnetic* and the last quadratic term is called *diamagnetic*. The quadratic term will here be neglected since it is commonly very small. For a particle with non-zero spin magnetic moment $\boldsymbol{\mu}_s$ an additional term equal to $-\boldsymbol{\mu}_s\cdot\boldsymbol{B}$ is present. The first order perturbation Hamiltonian for an electron in presence of an electromagnetic field can then be written as

$$H' = -e\phi + 2\frac{\mu_\mathrm{B}}{\hbar}(-i\hbar\boldsymbol{A}\cdot\nabla + \boldsymbol{s}\cdot\boldsymbol{B})\,,$$

where $\mu_\mathrm{B} = e\hbar/2m_\mathrm{e}$ is the Bohr magneton and it is assumed that the electronic g factor is exactly 2.

Zeeman effect

The vector potential of a homogeneous magnetic field is

$$\boldsymbol{A} = \frac{1}{2}(\boldsymbol{B}\times\boldsymbol{r})\,,$$

giving

$$-i\hbar\boldsymbol{A}\cdot\nabla = -i\hbar\frac{1}{2}(\boldsymbol{B}\times\boldsymbol{r})\cdot\nabla = -i\hbar\frac{1}{2}\boldsymbol{B}\cdot(\boldsymbol{r}\times\nabla) = -\frac{1}{2}\boldsymbol{B}\cdot\boldsymbol{l}\,,$$

since the operator $-i\hbar\boldsymbol{r}\times\nabla$ is equal to the $\boldsymbol{l}$ operator. The interaction between an electron and a homogeneous magnetic field, i.e., Zeeman effect, is thus described by

$$H_\mathrm{m} = \frac{\mu_\mathrm{B}}{\hbar}(\boldsymbol{l} + 2\boldsymbol{s})\cdot\boldsymbol{B}\,.$$

Hyperfine structure

The vector potential and field from a magnetic dipole are

$$\boldsymbol{A} = \frac{\mu_0}{4\pi}\frac{\boldsymbol{\mu}\times\boldsymbol{r}}{r^3}\,,\quad \boldsymbol{B} = \frac{\mu_0}{4\pi}\left[-\frac{\boldsymbol{\mu}}{r^3} + \frac{3\boldsymbol{r}(\boldsymbol{r}\cdot\boldsymbol{\mu})}{r^5} + \frac{8\pi}{3}\boldsymbol{\mu}\delta(\boldsymbol{r})\right]\,,$$

giving

$$-i\hbar\boldsymbol{A}\cdot\nabla = -i\hbar\frac{\mu_0}{4\pi}\frac{\boldsymbol{\mu}\times\boldsymbol{r}}{r^3}\cdot\nabla = -i\hbar\frac{\mu_0}{4\pi}\boldsymbol{\mu}\cdot\frac{\boldsymbol{r}\times\nabla}{r^3} = \frac{\mu_0}{4\pi}\frac{\boldsymbol{\mu}\cdot\boldsymbol{l}}{r^3}\,.$$

The interaction between a nuclear magnetic dipole $\boldsymbol{\mu}_I$ and an electron is thus described by

$$H_{\rm dip} = 2\frac{\mu_0}{4\pi}\frac{\mu_{\rm B}}{\hbar}\left[\frac{\boldsymbol{l}}{r^3} - \frac{\boldsymbol{s}}{r^3} + \frac{3(\boldsymbol{s}\cdot\boldsymbol{r})\boldsymbol{r}}{r^5} + \frac{2}{3}\frac{\delta(r)}{r^2}\boldsymbol{s}\right]\cdot\boldsymbol{\mu}_I$$

or

$$H_{\rm dip} = 2\frac{\mu_0}{4\pi}\frac{\mu_{\rm B}}{\hbar}\left[\frac{\boldsymbol{l}}{r^3} - \frac{\sqrt{10}\left\{\boldsymbol{s}\boldsymbol{C}^2\right\}^1}{r^3} + \frac{2}{3}\frac{\delta(r)}{r^2}\boldsymbol{s}\right]\cdot\boldsymbol{\mu}_I\,, \qquad \text{(B.2)}$$

by using spherical tensor notations.

B.2 Relativistic perturbation

The relativistic Dirac Hamiltonian for an electron in presence of an electromagnetic field is, in analogy with Eq. (B.1), given by

$$H = c\boldsymbol{\alpha}\cdot(-i\hbar\nabla + e\boldsymbol{A}) + \beta m_{\rm e}c^2 + V(\boldsymbol{r}) - e\phi$$

and the perturbation Hamiltonian for an electron in presence of an electromagnetic field can thus be written as

$$H' = -e\phi + ec\boldsymbol{\alpha}\cdot\boldsymbol{A}\,.$$

Zeeman effect

The vector potential of a homogeneous magnetic field gives

$$\boldsymbol{\alpha}\cdot\boldsymbol{A} = \frac{1}{2}(\boldsymbol{r}\times\boldsymbol{\alpha})\cdot\boldsymbol{B} = \frac{1}{2}r\left(\boldsymbol{C}^1\times\boldsymbol{\alpha}\right)\cdot\boldsymbol{B} = -i\sqrt{2}\frac{1}{2}r\left\{\boldsymbol{C}^1\boldsymbol{\alpha}\right\}^1\cdot\boldsymbol{B}\,,$$

since $\boldsymbol{r} = r\boldsymbol{C}^1$ and the vector product for tensor-operators of rank 1 is defined as $\boldsymbol{t}\times\boldsymbol{u} = -i\sqrt{2}\{\boldsymbol{t}\boldsymbol{u}\}^1$. The perturbation from the interaction with a homogeneous magnetic field is then described by

$$H_{\rm m} = -i\sqrt{2}\frac{ec}{2}r\left\{\boldsymbol{C}^1\boldsymbol{\alpha}\right\}^1\cdot\boldsymbol{B}\,.$$

Hyperfine structure

The vector potential from a magnetic dipole gives

$$\boldsymbol{\alpha}\cdot\boldsymbol{A}=\frac{\mu_0}{4\pi}\frac{\boldsymbol{r}\times\boldsymbol{\alpha}}{r^3}\cdot\boldsymbol{\mu}=\frac{\mu_0}{4\pi}\frac{\boldsymbol{C}^1\times\boldsymbol{\alpha}}{r^2}\cdot\boldsymbol{\mu}=-i\sqrt{2}\frac{\mu_0}{4\pi}\frac{\left\{\boldsymbol{C}^1\boldsymbol{\alpha}\right\}^1}{r^2}\cdot\boldsymbol{\mu}\,.$$

The interaction between a nuclear magnetic dipole $\boldsymbol{\mu}_I$ and an electron is thus described by

$$H_{\rm dip}=-i\sqrt{2}\frac{\mu_0}{4\pi}ec\frac{\left\{\boldsymbol{C}^1\boldsymbol{\alpha}\right\}^1}{r^2}\cdot\boldsymbol{\mu}\,. \tag{B.3}$$

B.3 General hyperfine operator

Hyperfine structure indicates a coupling between the electronic and nuclear angular momenta. The total angular momentum of the electrons, $\boldsymbol{J}$, and the nucleus, $\boldsymbol{I}$, respectively, couple to form a total angular momentum $\boldsymbol{F}$, given by

$$\boldsymbol{F}=\boldsymbol{J}+\boldsymbol{I}$$

with the quantum numbers

$$\begin{aligned} F &= J+I, J+I-1, \ldots, |J-I| \\ M_F &= F, F-1, \ldots, -F\,. \end{aligned}$$

Generally, the perturbation from the interaction between electrons and nuclear multipole fields can be written in terms of scalar products of spherical tensor operators:

$$H_{\rm hfs}=\sum_{k=1}^{\infty}\boldsymbol{T}^k\cdot\boldsymbol{M}^k\,, \tag{B.4}$$

where $\boldsymbol{M}^k$ represents the 2^k moment of the nucleus and $\boldsymbol{T}^k$ the corresponding electronic field at the nucleus. For parity reasons, magnetic interactions give rise only to odd k (dipole, octupole, ...) and electric interactions only to even k (quadrupole, hexadecapole, ...), i.e., for $k=1$ we have $\boldsymbol{M}^1=\boldsymbol{\mu}$ and get the magnetic dipole interaction above and for the case of $k=2$ we have $\boldsymbol{M}^2=\boldsymbol{Q}^2$ and get the electric quadrupole interaction etc. The electronic tensor operators $\boldsymbol{T}^k$ are one-body operators for many-electron systems and can be rewritten in terms of sums of single-electron operators:

$$\boldsymbol{T}^k=\sum_{i=1}^{N}\boldsymbol{t}_i^k\,.$$

For $k = 1$ the non-relativistic $\boldsymbol{t}$ operator can be found by identification with Eq. (B.2):

$$\boldsymbol{t}^1 = 2\frac{\mu_0}{4\pi}\frac{\mu_\mathrm{B}}{\hbar}\left[\frac{\boldsymbol{l}}{r^3} - \frac{\sqrt{10}\left\{\boldsymbol{C}^2\boldsymbol{s}\right\}^1}{r^3} + \frac{2}{3}\frac{\delta(r)}{r^2}\boldsymbol{s}\right] .$$

The general relativistic $\boldsymbol{t}$ operators are given by the following expressions

$$\boldsymbol{t}^k = \begin{cases} -\dfrac{e}{4\pi\epsilon_0}\dfrac{\boldsymbol{C}^k}{r^{k+1}} & \text{for } k \text{ even}\,, \\ -i\dfrac{\mu_0}{4\pi}ec\left(\dfrac{k+1}{k}\right)^{1/2}\dfrac{\left\{\boldsymbol{C}^k\boldsymbol{\alpha}\right\}^k}{r^{k+1}} & \text{for } k \text{ odd}\,. \end{cases}$$

It is easily shown that these expressions in combination with Eq. (B.4) for $k = 1$ gives the relativistic expression for the hyperfine dipole interaction, i.e., Eq. (B.3).

B.4 Matrix elements of the hyperfine operator

The matrix element of the general hyperfine operator (B.4) is

$$\begin{aligned} \langle\psi|H_\mathrm{hfs}|\psi'\rangle &= \sum_k N\langle\gamma_J\gamma_I(JI)FM_F|\boldsymbol{T}^k\cdot\boldsymbol{M}^k|\gamma'_J\gamma_I(J'I)F'M'_F\rangle \\ &= N(-1)^{J'+I+F}\delta(F,F')\delta(M_F,M'_F) \\ &\quad \sum_k \left\{\begin{array}{ccc} J & I & F \\ I & J' & k \end{array}\right\}\langle\gamma_J J||\boldsymbol{T}^k||\gamma'_J J'\rangle\langle\gamma_I I||\boldsymbol{M}^k||\gamma_I I\rangle\,, \end{aligned}$$

where N is a normalizing constant. The matrix elements diagonal with respect to J and I give the energy shift due to the hyperfine interaction:

$$E_\mathrm{hfs} = N(-1)^{J+I+F}\sum_k \left\{\begin{array}{ccc} J & I & F \\ I & J & k \end{array}\right\}\langle\gamma_J J||\boldsymbol{T}^k||\gamma_J J\rangle\langle\gamma_I I||\boldsymbol{M}^k||\gamma_I I\rangle\,.$$

In the case of dipole interaction $k = 1$ have these diagonal matrix element the same F dependence as the scalar product $\boldsymbol{J}\cdot\boldsymbol{I}$:

$$\langle(JI)FM_F|\boldsymbol{J}\cdot\boldsymbol{I}|(JI)FM_F\rangle = (-1)^{J+I+F}\left\{\begin{array}{ccc} J & I & F \\ I & J & 1 \end{array}\right\}\langle J||\boldsymbol{J}||J\rangle\langle I||\boldsymbol{I}||I\rangle\,.$$

Hence, can the energy shift E_dip be produced by replacing the dipole operator, given by Eq. (B.2) or (B.3), with the *"equivalent" operator*

$$H_\mathrm{dip} = \frac{A}{\hbar^2}\boldsymbol{J}\cdot\boldsymbol{I}\,,$$

where

$$A = \frac{\langle \gamma_J J||\boldsymbol{T}^1||\gamma_J J\rangle\langle \gamma_I I||\boldsymbol{\mu}_I||\gamma_I I\rangle}{\langle J||\boldsymbol{J}||J\rangle\langle I||\boldsymbol{I}||I\rangle}\hbar^2\,.$$

This A factor is called the *dipole interaction constant*. The F dependence of the dipole energy shift can easily be obtained from the 6-j symbol or by using the identity

$$\boldsymbol{J}\cdot\boldsymbol{I} = \frac{1}{2}(\boldsymbol{F}^2 - \boldsymbol{J}^2 - \boldsymbol{I}^2)\,,$$

giving

$$E_{\rm dip} = \frac{A}{2}[F(F+1) - J(J+1) - I(I+1)]\,.$$

where the separation between the levels F and $F-1$ is

$$\Delta E_{\rm dip} = AF\,.$$

Furthermore, it can be assumed that the nuclear wavefunction is normalized but the electronic is not, the A-factor can then be rewritten as

$$A = \frac{\langle \gamma_J J||\boldsymbol{T}^1||\gamma_J J\rangle}{N[J(J+1)(2J+1)]^{1/2}}g_I\mu_{\rm N}\,,$$

since

$$\langle J||\boldsymbol{J}||J\rangle = N\hbar[J(J+1)(2J+1)]^{1/2}$$

and the nuclear matrix element in the numerator by definition is

$$\langle \gamma_I I||\boldsymbol{\mu}_I||\gamma_I I\rangle = g_I\frac{\mu_{\rm N}}{\hbar}\langle I||\boldsymbol{I}||I\rangle\,.$$

The electronic wavefunctions are here supposed to be perturbed and not necessarily normalized, but the energy shift can also be expressed by means of a corresponding *"effective"* operator and *unperturbed* (and normalized) wavefunctions. Moreover, for the one-electron systems considered in this thesis the effective dipole operator is equal to the dipole operators given by Eqs. (B.2) and (B.3).

A s-state of a hydrogen-like system with non-zero I is split into two sublevels with $F = I+1/2$ and $F = I-1/2$, respectively due to the hyperfine dipole interaction. The *non-relativistic* A-factor in this case becomes

$$A = \frac{4}{3}\frac{\mu_0}{4\pi}\mu_{\rm B}\int_0^\infty P_{ns}\frac{\delta(r)}{r^2}P_{ns}{\rm d}r = \frac{16}{3}\frac{\mu_0}{4\pi}\mu_{\rm B}\frac{Z^3}{n^3a_0^3}g_I\mu_{\rm N} = \frac{4}{3}\alpha^4 m_{\rm e}c^2\frac{Z^3}{n^3}g_I\frac{m_{\rm e}}{m_{\rm p}}\,,$$

where $a_0 = 4\pi\epsilon_0\hbar^2/m_e e^2$ is the Bohr radius, giving an energy separation of

$$\Delta E = \frac{4}{3}\alpha^4 m_e c^2 \frac{Z^3}{n^3} g_I \frac{m_e}{m_p}\left(I + \tfrac{1}{2}\right) .$$

The corresponding *relativistic* expressions are

$$A = \frac{8}{3}\frac{\mu_0}{4\pi} e c g_I \mu_N \int_0^\infty F_{ns}\frac{1}{r^2}G_{ns}\mathrm{d}r = \frac{8}{3}\frac{e}{4\pi\epsilon_0 c} g_I \mu_N \int_0^\infty F_{ns}\frac{1}{r^2}G_{ns}\mathrm{d}r$$

and

$$\Delta E = \frac{8}{3}\frac{e}{4\pi\epsilon_0 c} g_I \mu_N \left(I + \tfrac{1}{2}\right) \int_0^\infty F_{ns}\frac{1}{r^2}G_{ns}\mathrm{d}r\,.$$

These expressions hold for point-like nuclear magnetizations, corrections for the extended magnetization lead to the Bohr-Weisskopf effect, as discussed in Sec. 3.2.

APPENDIX C

The Nuclear Magnetic Dipole Moment in ^{207}Pb

The nuclear magnetic moment of ^{207}Pb has been of some concern recently, in connection with the measurements of the hfs of the hydrogen-like ion at GSI. The compilation by Raghavan [59] lists two different experimental values: The NMR value 0.592 583(9) $\mu_{\rm N}$, by Lutz and Stricker [60] and the optical pumping value, 0.582 19(2) $\mu_{\rm N}$, by Gibbs and White [61], differing by 1.8%, well outside the claimed relative accuracies of 1.5×10^{-5} and 3.4×10^{-5}, respectively. This discrepancy clearly affects the comparison between experimental and theoretical results for the 1s hyperfine structure.

There have been several attempts to reduce the discrepancy and we give below a short review of the work performed during the last decades. It must be emphasized that a magnetic shielding (diamagnetic shielding and possible chemical shift) is present in all measurements of nuclear magnetic dipole moments. To allow for this effect the observed nuclear magnetic dipole moment must thus be multiplied by a $(1-\sigma)^{-1}$, where σ is the magnetic shielding factor. Diamagnetic shielding factors $\sigma_{\rm a}$ for atomic systems can be calculated with sufficient accuracy as also discussed in Paper IV. A value of the nuclear magnetic dipole moment which is not corrected for the magnetic shielding is called *uncorrected*, and will be denoted by μ_I', to differ from the *corrected* (or bare) value μ_I.

The tabulation by Lindgren [49] gives a clear presentation of the corrections and difficulties involved in the determination of nuclear magnetic moments. The tabulation lists an NMR value by Proctor for the uncorrected

nuclear magnetic dipole moment of ^{207}Pb:

$$\mu'_I = 0.583\,65(8)\ \mu_{\rm N}$$

as reported in 1950 [62] from a measurement on $Pb(C_2H_3O_2)_2$. It must be emphasized that the uncertainty of this value and the moments below do not include the uncertainty in the shielding correction unless otherwise is specifically stated.

This NMR value of Proctor is also listed in the compilation by Fuller [63] together with other NMR results determined in the 1950s. The other results were determined for various chemical compounds giving in chemical shifts up to 0.21%. A 1969 optical pumping experiment in the $^3P_0$ ground state of free ^{207}Pb atoms by Gibbs and White [61] resulted in an observed nuclear resonance corresponding to

$$\mu'_I = 0.572\,35(2)\ \mu_{\rm N}\,.$$

This result deviates from the Proctor value by 2% and is said to corroborate "very large chemical shifts of 2–3% in essentially all Pb compounds used to date for NMR investigations". This interpretation of the discrepancy was supported by an article by Lutz and Stricker [60], who in 1971 reported their NMR experiment as a measurement of "the shielding of lead ions by water". This measurement was carried out on $Pb(NO_3)_2$ in heavy water resulting in

$$\mu'_I = 0.582\,543(9)\ \mu_{\rm N}.$$

after an extrapolation to vanishing concentration of lead nitrate. The difference of $-1.78(1)$% between the optical pumping value and this NMR result was interpreted as a shielding of the ^{207}Pb nucleus in the Pb^{2+} ion by D_2O and reported as the main result by Lutz and Stricker. The optical pumping value and the NMR value in the compilation by Raghavan originates from the work by Gibbs and White and by Lutz and Stricker, respectively.

However, in 1970 Margerie [64] pointed out that the $^3P_0$ term of the $6p^2$ ground state configuration in the Pb atom gets an admixture of the $^3P_1$ term of the same configuration due to hyperfine interaction. This admixture would affect an optical pumping experiment on the ground state and can thus explain the large difference between the Gibbs value and the (Proctor) NMR value. The nuclear magnetic dipole moment can then be written as

$$\mu'_I = \mu(^3\tilde{\rm P}_0) - \delta\mu(^3\tilde{\rm P}_0)\,,$$

where $\mu(^3\tilde{\rm P}_0)$ is the magnetic dipole moment of the mixted $^3P_0$ term (measured by Gibbs and White) and $\delta\mu(^3\tilde{\rm P}_0)$ is a correction due to the admixture.

Margerie calculated the correction to be $-0.0068(29)\ \mu_{\rm N}$, corresponding to a nuclear magnetic dipole moment of

$$\mu_I' = 0.5791(29)\ \mu_{\rm N}\,,$$

which almost coincides with the NMR value. The compilation by Fuller [63] quotes a 1972 private communication by Gibbs noting that "large discrepancy with NMR-value may be due to large interaction of $^3P_1$-state with $^3P_0$-state". In 1978 Sushkov *et al.* [65] observed that the expressions used by Margerie were very sensitive to small corrections. Sushkov *et al.* used a different, less sensitive expression. They solved the Dirac equation numerically in a parameterized potential, where the parameters were optimized to fit the terms of the ground configuration, including the fine structure. They then included admixtures of the type $6p \rightarrow np$, and obtained a mixing parameter by fitting the hyperfine splitting constants for the $6p^2$ states of Pb. Using relativistic correction factors equivalent "with an accuracy to within notations" to the expressions by Margerie they obtained $-0.0118\ \mu_{\rm N}$. Their article contains no estimation of the uncertainty in the correction term, but assuming a relative uncertainty of 10% seems to reasonable from their discussion. Their value for nuclear magnetic dipole moment would then be

$$\mu_I' = 0.5842(12)\ \mu_{\rm N}\,,$$

in even better agreement with the NMR value. Even this calculation includes only a limited amount of correlation effects, and could probably be improved with more powerful computing techniques.

In 1988 Brenner reported of high-frequency measurements on the $^3P_1$ term of the ground-state configuration for ^{207}Pb with use of the ABMR technique [66]. A combined analysis of his data with the results of Gibbs and White gave an estimate of the mixing of the fine-structure levels due to the hyperfine interaction. A correction term to the optical pumping result for the nuclear magnetic dipole moment could then be estimated to be $-0.0073(14)\ \mu_{\rm N}$, corresponding to a nuclear magnetic dipole moment of

$$\mu_I' = 0.5797(14)\ \mu_{\rm N}\,.$$

In general, a comparison between nuclear magnetic moments obtained by different methods requires that the moments are corrected for magnetic shielding, which depends on the configuration and environment. The diamagnetic corrections used in Paper IV for different charge states of atomic PB were taken from Johnson and co-workers based on RHFS and RPA calculations [67–71], giving:

$$\begin{array}{ll} \text{neutral Pb} & (1-\sigma_{\rm a})^{-1} = 1.020\,98(21)\ , \\ \text{Pb}^{2+} & (1-\sigma_{\rm a})^{-1} = 1.017\,02(6)\ . \end{array}$$

The diamagnetic correction for the Pb^{2+} ion and an assumed relative uncertainty of 2×10^{-3} due to the chemical shift, motivated by the differences among the NMR values, yields

$$\mu_I = 0.5925(12)\ \mu_{\rm N}$$

as the *corrected NMR value* of Lutz and Stricker. The following *corrected optical pumping values*:

$$\begin{array}{ll} \text{Gibbs and White:} & \mu_I = 0.584\,36(12)\ \mu_{\rm N} \\ \text{Sushkov } \textit{et al.}\text{:} & \mu_I = 0.5942(12)\ \mu_{\rm N} \\ \text{Brenner} & \mu_I = 0.5918(14)\ \mu_{\rm N} \end{array}$$

were yielded by using the diamagnetic correction for neutral Pb on the values by Gibbs and White and Brenner, and by using the diamagnetic correction for the Pb^{2+} ion on the value by Sushkov *et al.*. The advantages and disadvantages of these four corrected values can be summarized as:

- the NMR value by Lutz and Stricker is subject to an unknown chemical shift which, however, is only due to surrounding heavy water molecules,
- the optical pumping value by Gibbs and White was performed on free atoms, but the original result did not take the mixing of $^3P_0$ and $^3P_1$ into account,
- the theoretical work by Sushkov *et al.* gives a correction to the value by Gibbs and White, and includes a limited amount of correlation,
- the ABMR measurements by Brenner also produces a correction to the value by Gibbs and White, however with a relative large uncertainty.

The result of our analysis is that the nuclear magnetic dipole moment of ^{207}Pb is associated with a considerable uncertainty, at least of the order of 0.2%, and thus that the accuracy indicated in the NMR value tabulated by Raghavan is considerably overestimated. To obtain a value for the nuclear magnetic moment with higher accuracy, a more precise ABMR measurement would be helpful, as would a renewed analysis of optical pumping as well as ABMR results, using more complete atomic wavefunctions. This uncertainty concerning the Pb magnetic moment presents, of course, a serious complication in the interpretation of the accurate measurements of the 1s hyperfine structure in H-like Pb.

Bibliography

[1] W. Pauli, jr. Zur Frage der theoretischen Deutung der Satelliten einiger Spektrallinien und ihrer Beeinflussung durch magnetische Felder. *Die Naturwissenschaften*, 12(37):741–743, 1924.

[2] S. Goudsmit and E. Back. Feinstrukturen und Termordnung des Wismutspektrums. *Zeitschrift für Physik*, 43(5–6):321–334, 1927.

[3] H. Schüler. Über die Struktur der gelben Na-Linien (5890, 5896). *Die Naturwissenschaften*, 16(25):512–513, 1928.

[4] D. A. Jackson. Hyperfine Structure in the Arc Spectrum of Cæsium and Nuclear Rotation. *Proceedings of the Royal Society of London, Series A*, 121(787):432–447, 1928.

[5] A. Filippov and E. Gross. Feinstruktur der Hauptseriendublets des Caesiums und des Rubidiums. *Die Naturwissenschaften*, 17(7):121, 1929.

[6] E. Fermi. Über die magnetischen Momente der Atomkerne. *Zeitschrift für Physik*, 60(5–6):320–333, 1930.

[7] Douglas R. Hartree. *The Calculation of Atomic Structures*. John Wiley & Sons, New York, 1957.

[8] H. Kopfermann. *Nuclear Moments*. Academic Press, New York, 1958.

[9] Norman F. Ramsey. Experiments with separated oscillatory fields and hydrogen masers. *Reviews of Modern Physics*, 62(3):541–552, 1990.

[10] Bernhard Franzke. The heavy ion storage and cooler ring project ESR at GSI. *Nuclear Instruments and Methods in Physics Research*, B24/25:18–25, 1987.

[11] D. A. Knapp, R. E. Marrs, S. R. Elliot, E. W. Magee, and R. Zasadzinski. A high-energy electron beam ion trap for production of high-charge high-Z ions. *Nuclear Instruments and Methods in Physics Research A*, 334(2,3):305–312, 1993.

[12] José R. Crespo López-Urrutia, P. Beiersdorfer, Daniel W. Savin, and Klaus Widmann. Direct Observation of the Spontaneous Emission of the Hyperfine Transition $F = 4$ to $F = 3$ in Ground State Hydrogenlike $^{165}Ho^{66+}$ in an Electron Beam Ion Trap. *Physical Review Letters*, 77(5):826–829, 1996.

[13] P. Seelig, S. Borneis, A. Dax, T. Engel, S. Faber, M. Gerlach, C. Holbrow, G. Huber, T. Kühl, D. Marx, K. Meier, P. Merz, W. Quint, F. Schmitt, M. Tomaselli, L. Völker, H. Winter, M. Würtz, K. Beckert, B. Franzke, F. Nolden, H. Reich, M. Steck, and T. Winkler. Ground State Hyperfine Splitting of Hydrogenlike $^{207}Pb^{81+}$ by Laser Excitation of a Bunched Ion Beam in the GSI Experimental Storage Ring. *Physical Review Letters*, 81(22):4824–4827, 1998.

[14] I. Klaft, S. Borneis, T. Engel, B. Fricke, R. Grieser, G. Huber, T. Kühl, D. Marx, R. Neumann, S. Schröder, P. Seelig, and L. Völker. Precision Laser Spectroscopy of the Ground State Hyperfine Splitting of Hydrogenlike $^{209}Bi^{82+}$. *Physical Review Letters*, 73(18):2425–2427, 1994.

[15] P. Beiersdorfer, A. L. Osterheld, J. H. Scofield, J. R. Crespo López-Urrutia, and K. Widmann. Measurement of QED and Hyperfine Splitting in the $2s_{1/2}$-$2p_{3/2}$ X-Ray Transition in Li-like $^{209}Bi^{80+}$. *Physical Review Letters*, 80(14):3022–3025, 1998.

[16] H. Persson, S. M. Schneider, W. Greiner, G. Soff, and I. Lindgren. Self-Energy Correction to the Hyperfine Structure Splitting of Hydrogenlike Atoms. *Physical Review Letters*, 76(9):1433–1436, 1996.

[17] P. Sunnergren, H. Persson, S. Salomonson, S. M. Schneider, I. Lindgren, and G. Soff. Radiative corrections to the hyperfine-structure splitting of hydrogenlike systems. *Physical Review A*, 58(2):1055–1069, 1998.

[18] V. M. Shabaev, M. Tomaselli, T. Kühl, A. N. Artemyev, and V. A. Yerokhin. Ground-state hyperfine splitting of high-Z hydrogenlike ions. *Physical Review A*, 56(1):252–255, 1997.

[19] S. A. Blundell, K. T. Cheng, and J. Sapirstein. Radiative corrections in atomic physics in the presence of perturbing potentials. *Physical Review A*, 55(3):1857–1865, 1997.

[20] Hermann Haken and Hans Christoph Wolf. *The Physics of Atoms and Quanta*. Springer-Verlag, Berlin, 5th edition, 1996.

[21] I. Lindgren and J. Morrison. *Atomic Many-Body Theory*, volume 3 of *Springer Series on Atoms + Plasmas*. Springer-Verlag, Berlin, 2nd edition, 1986.

[22] J. J. Sakurai. *Advanced Quantum Mechanics*. Addison-Wesley, Reading, 1967.

[23] Norman F. Ramsey. *Molecular Beams*. Oxford University Press, Oxford, 1956.

[24] Lloyd Armstrong, Jr. *Theory of the Hyperfine Structure of Free Atoms*. John Wiley & Sons, New York, 1971.

[25] Charlotte Froese Fischer. *The Hartree-Fock Method for Atoms*. John Wiley & Sons, New York, 1977.

[26] J.-L. Heully, I. Lindgren, E. Lindroth, and A.-M. Mårtensson-Pendrill. Comment on relativistic wave equations and negative-energy states. *Physical Review A*, 33(6):4426–4429, 1986.

[27] Sten Salomonson and Per Öster. Relativistic all-order pair functions from a discretized single-particle Dirac Hamiltonian. *Physical Review A*, 40(10):5548–5558, 1989.

[28] Sten Salomonson and Per Öster. Solution of the pair equation using a finite discrete spectrum. *Physical Review A*, 40(10):5559–5567, 1989.

[29] Ingvar Lindgren, Hans Persson, Sten Salomonson, and Leonti Labzowsky. Full QED calculations of two-photon exchange for heliumlike-systems: Analysis in the Coulomb and Feynman gauges. *Physical Review A*, 51(2):1167–1195, 1995.

[30] Hans Persson, Sten Salomonson, Per Sunnergren, and Ingvar Lindgren. Two-Electron Lamb-Shift Calculations on Heliumlike Ions. *Physical Review Letters*, 76(2):204–207, 1996.

[31] P. Petit, M. Desaintfuscien, and C. Audoin. Temperature Dependence of the Hydrogen Maser Wall Shift in the Temperature Range 295–395 K. *Metrologia*, 16(1):7–14, 1980. Addendum in Metrologia 16(4):184, 1980.

[32] Guiseppe Cocconi and Philip Morrison. Searching for Interstellar Communications. *Nature (London)*, 184(4690):844–846, 1959.

[33] P. Pyykkö, E. Pajanne, and Mitio Inokuti. Hydrogen-Like Relativistic Corrections for Electric and Magnetic Hyperfine Integrals. *International Journal of Quantum Chemistry*, VII(4):785–806, 1973.

[34] Jenny E. Rosenthal and G. Breit. The Isotope Shift in Hyperfine Structure. *Physical Review*, 41(4):459–470, 1932.

[35] M. F. Crawford and A. K. Schawlow. Electron-Nuclear Potential Fields from Hyperfine Structure. *Physical Review*, 76(9):1310–1317, 1949.

[36] H. J. Rosenberg and H. H. Stroke. Effects of a Diffuse Nuclear Charge Distribution on the Hyperfine-Structure Interaction. *Physical Review A*, 5(5):1992–2000, 1972.

[37] V. M. Shabaev. Hyperfine structure of hydrogen-like ions. *Journal of Physics B*, 27(24):5825–5832, 1994.

[38] H. de Vries, C. W. de Jager, and C. de Vries. Nuclear Charge-Density-Distribution Parameters from Elastic Electron Scattering. *Atomic Data and Nuclear Data Tables*, 36(3):495–536, 1987.

[39] G. Fricke, C. Bernhardt, K. Heilig, L. A. Schaller, L. Schellenberg, E. B. Schera, and C. W. de Jager. Nuclear Ground State Charge Radii from Electromagnetic Interactions. *Atomic Data and Nuclear Data Tables*, 60(2):177–285, 1995.

[40] Aage Bohr and V. F. Weisskopf. The Influence of Nuclear Structure on the Hyperfine Structure of Heavy Elements. *Physical Review*, 77(1):94–98, 1950.

[41] Aage Bohr. Nuclear Magnetic Moments and Atomic Hyperfine Structure. *Physical Review*, 81(3):331–335, 1951.

[42] Christian Forssén. Hyperfine Structure — A Bridge between Nuclear and Atomic Physics. Master's thesis, Physics and Engineering Physics, Göteborg University and Chalmers University of Technology, 1998.

[43] L. N. Labzowsky, W. R. Johnson, G. Soff, and S. M. Schneider. Dynamic proton model for the hyperfine structure of the hydrogenlike ion $^{209}_{83}\mathrm{Bi}^{82+}$. *Physical Review A*, 51(6):4597–4602, 1995.

[44] M. Tomaselli, S. M. Schneider, E. Kankeleit, and T. Kühl. Ground-state magnetization of ^{209}Bi in a dynamic-correlation model. *Physical Review C*, 51(6):2989–2997, 1995.

[45] M. Tomaselli, T. Kühl, P. Seelig, C. Holbrow, and E. Kankeleit. Hyperfine splittings of hydrogenlike ions and the dynamic-correlation model for one-hole nuclei. *Physical Review C*, 58(3):1524–1534, 1998.

[46] F. Mandl and G. Shaw. *Quantum Field Theory*. John Wiley & Sons, New York, 1984.

[47] Micheal E. Peskin and Daniel V. Schroeder. *An Introduction to Quantum Field Theory*. Addison-Wesley, Reading, 1995.

[48] Per Sunnergren. *Complete One-Loop QED Calculations for Few-Electron Ions — Applications to Electron-Electron Interaction, the Zeeman effect and Hyperfine Structure*. PhD thesis, Physics and Engineering Physics, Göteborg University and Chalmers University of Technology, 1998.

[49] Ingvar Lindgren. Analysis of nuclear dipole moments determined with nuclear magnetic resonance. *Arkiv för Fysik*, 29(44):553–563, 1965.

[50] T. William Donnelly and Ingo Sick. Elastic magnetic electron scattering from nuclei. *Reviews of Modern Physics*, 56(3):461–566, 1984.

[51] E. Rost. Proton shell-model potentials for lead and the stability of superheaby nuclei. *Physics Letters*, 26B(4):184–187, 1968.

[52] V. M. Shabaev, M. B. Shabaeva, I. I. Tupitsyn, V. A. Yerokhin, A. N. Artemyev, T. Kühl, M. Tomaselli, T. Kühl, and O. M. Zherebtsov. Transition energy and lifetime for the ground-state hyperfine splitting of high-Z lithiumlike ions. *Physical Review A*, 57(1):149–156, 1998.

[53] A. Lurio and A. G. Prodell. Hfs Separations and Hfs Anomalies in the $^2P_{1/2}$ State of Ga^{69}, Ga^{71}, Tl^{203}, and Tl^{205}. *Physical Review*, 101(1):79–83, 1956.

[54] Edward B. Baker and L. W. Burd. Frequency-Swept and Proton-Stabilized NMR Spectrometer for all Nuclei Using a Frequency Synthesizer. *Review of Scientific Instruments*, 34(3):238–243, 1963.

[55] Ann-Marie Mårtensson-Pendrill. Magnetic Moment Distributions in Tl Nuclei. *Physical Review Letters*, 74(12):2184–2187, 1995.

[56] R. Engfer, H. Schneuwly, J. L. Vuilleumier, H. K. Walter, and A. Zehnder. Charge-Distribution Parameters, Isotope shifts, Isomer shifts, and Magnetic Hyperfine Constants from Muonic Atoms. *Atomic Data and Nuclear Data Tables*, 14(5–6):509–597, 1974.

[57] John David Jackson. *Classical Electrodynamics*. John Wiley & Sons, New York, 2nd edition, 1975.

[58] Ingvar Lindgren and Arne Rosén. Relativistic self-consistent-field calculations with application to atomic hyperfine interaction, Part II: Relativistic theory of atomic hyperfine interaction. *Case Studies in Atomic Physics*, 4(3):150–196, 1974.

[59] Pramila Raghavan. Table of Nuclear Moments. *Atomic Data and Nuclear Data Tables*, 42(2):189–291, 1989.

[60] O. Lutz and G. Stricker. The magnetic moment of ^{207}Pb and the shielding of lead ions by water. *Physics Letters*, 35A(6):397–398, 1971.

[61] Hyatt M. Gibbs and C. M. White. Polarization of Pb Vapour. II. Disorientation of Pb^{207} Ground State and $\mu_I(Pb^{207})/\mu_I(Hg^{199})$. *Physical Review*, 188(1):180–187, 1969.

[62] W. G. Proctor. On the Magnetic Moments of Tl^{203}, Tl^{205}, Sn^{115}, Sn^{117}, Sn^{119}, Cd^{111}, Cd^{113}, and Pb^{207}. *Physical Review*, 79(1):35–44, 1950.

[63] Gladys H. Fuller. Nuclear Spins and Moments. *Journal of Physical and Chemical Reference Data*, 5(4):835–1092, 1976.

[64] Jean Margerie. Facteurs de Landé des niveaux $6p^2\ ^3P_0$ et $6p^2\ ^1S_0$ de ^{207}Pb. *Comptes rendus hebdomadaires des séances de l'Académie des sciences, Série B: Sciences physiques*, 271(1):209–212, 1970.

[65] O. P. Sushkov, V. V. Flambaum, and I. B. Khriplovich. Theory of hyperfine structure of heavy atoms. *Optics and Spectroscopy*, 44(1):2–6, 1978. Russian original: *Optika i Spektroskopija*, 44(1):3–11, 1978.

[66] Thomas Brenner. *Hochfrequenzspektroskopische Messungen an den Zuständen der Grundzustandkonfiguration $6s^2 6p^2$ von ^{208}Pb und ^{207}Pb.* PhD thesis, Institut für Angewandte Physik der Rheinischen Friedrich-Wilhelms-Universität Bonn, 1988.

[67] F. D. Feiock and W. R. Johnson. Relativistic Evaluation of Internal Diamagnetic Fields for Atoms and Ions. *Physical Review Letters*, 21(12):785–786, 1968.

[68] F. D. Feiock and W. R. Johnson. Atomic Susceptibilities and Shielding Factors. *Physical Review*, 187(1):39–50, 1969.

[69] Dietmar Kolb, W. R. Johnson, and Philip Shorer. Electric and magnetic susceptibilities and shielding factors for closed-shell atoms and ions of high nuclear charge. *Physical Review A*, 26(1):19–31, 1982.

[70] W. R. Johnson, Dietmar Kolb, and K.-N. Huang. Electric-Dipole, Quadrupole, and Magnetic-Dipole Susceptibilities and Shielding Factors for Closed-Shell Ions of the He, Ne, Ar, Ni (Cu^+), Kr Pb, and Xe Isoelectronic Sequences. *Atomic Data and Nuclear Data Tables*, 28(2):333–340, 1983.

[71] Walter R. Johnson. Private communication, 1998.

På grund av upphovsrättsliga skäl kan vissa ingående delarbeten ej publiceras här.
För en fullständig lista av ingående delarbeten, se avhandlingens början.

Due to copyright law limitations, certain papers may not be published here.
For a complete list of papers, see the beginning of the dissertation.

GÖTEBORGS UNIVERSITET

Paper I

Paper II

Paper III

Paper IV

Paper V

Paper VI

Paper VII